The design of transcription factor-based inhibitors to target Myc: drop the Myc!

Ellenbroek, B.D.

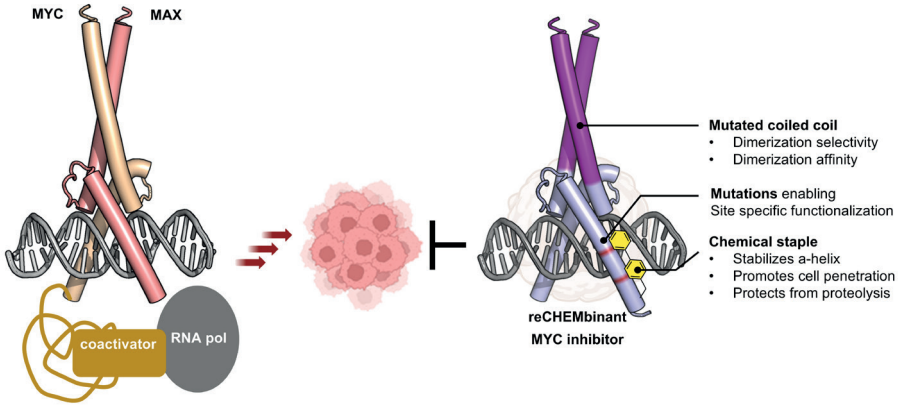

Adapted from: J. P. Kahler, B. D. Ellenbroek, V. E. van der Noord, B. van de Water, S. J. Pomplun, "ReCHEMbinant stapling enhances intracellular delivery and bioactivity of engineered protein inhibitors" *Chem* 2025, 102839.

The data not included in this thesis (uncut gels and list of differently expressed genes) can be found here: https://doi.org/10.1016/j.chempr.2025.102839

Chapter 4

ReCHEMbinant Stapling Enhances Intracellular Delivery and Bioactivity of Engineered Protein Inhibitors

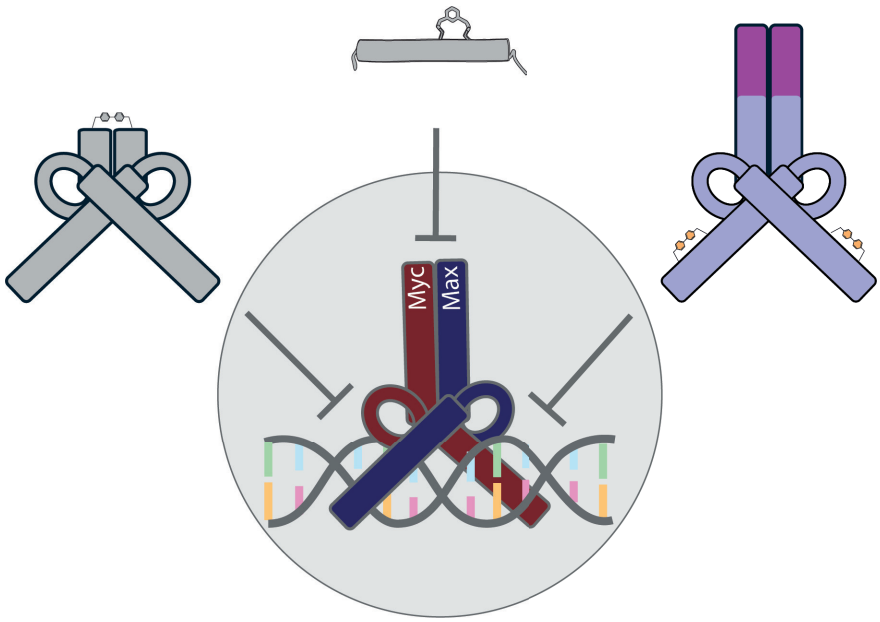

Authors:

Jan Pascal Kahler, **Brecht D. Ellenbroek**, Vera E. van der Noord, Bob van de Water, Sebastian J. Pomplun

Abstract

Protein therapeutics have transformed drug discovery by enabling modulation of challenging targets inaccessible to small molecules. However, most proteins lack the ability to penetrate cells, where many critical drug targets reside. Here, we present reCHEMbinant protein engineering, a strategy designed to generate synthetically enhanced proteins with improved structural stability, serum resistance, and cellular uptake. Applying this approach to Omomyc, a protein-based MYC inhibitor, we developed several reCHEMbinant stapled variants (HeloMYCs) exhibiting low-nanomolar DNA-binding affinity. Notably, the i, i+7 biphenyl-stapled construct HeloMYC-1421 outperformed Omomyc across several functional assays, including potent inhibition of MYC-driven gene expression in luciferase reporter assays and selective antiproliferative effects in MYC-dependent cells. Live-cell imaging showed that these enhanced effects result from significantly improved cellular uptake. Transcriptional reprogramming was further confirmed by RNA-seq. Together, our findings establish reCHEMbinant engineering as a chemically defined strategy for stapling entire recombinant proteins to enhance their intracellular bioactivity.

4.1 Introduction

Protein therapeutics have revolutionized drug discovery and expanded treatment options for challenging diseases.[1] With the advent of recombinant technology, protein drugs have enabled the targeting of drug targets previously elusive for small molecules.[2] Notable examples include antibodies like Herceptin[3] and Keytruda,[4] as well as other therapeutic proteins such as erythropoietin (EPO)[5] and interferon. [6] Due to their complex structures and extensive surfaces, protein drugs can recognize their targets with high specificity and potency. However, their large size and physicochemical properties prevent them from entering cells, making them effective primarily for extracellular targets. Many compelling drug targets, including thousands of protein-protein interactions (PPIs) and protein-nucleic acid interactions (PNAIs) do, however, reside inside cells, making them hardly accessible for protein based drugs.[7,8]

Strategies that enable the direct cytosolic delivery of therapeutic proteins would have transformative potential for targeting intracellular pathways. Traditional approaches have relied on fusion to cell-penetrating peptides (CPPs), such as cyclic polyarginines, to facilitate uptake.[9–11] These methods have enabled the delivery of cargos like nanobodies[9] and ubiquitin[10] into cells, primarily in model systems. However, CPPs often exhibit nonspecific toxicity and poor serum stability, limiting their translational potential. An alternative approach developed by the Raines group involves transient masking of surface-exposed carboxylates as esters to promote protein uptake, demonstrated using GFP.[12,13] While conceptually elegant, this strategy is hampered by the serum lability of esters, which precludes therapeutic application. Other efforts have focused on miniaturizing protein domains into proteomimetic peptides that mimic key binding motifs.[14–18] These constructs are often stabilized by chemical linkers or hydrocarbon staples and can achieve enhanced cell permeability thanks to their decreased size. However, replacing full-length proteins with short peptides can lead to reduced affinity or specificity, particularly when the target recognition depends on complex tertiary structures.

We sought to investigate a more general strategy for intracellular protein delivery by directly modifying full-length recombinant proteins. Our approach combines rationally introduced point mutations with compact, stable chemical modifications to enhance structural integrity and promote cell permeability, without relying on large fusion tags or inherently toxic motifs.

For studies, we selected Omomyc, a well-characterized, dominant-negative variant of the transcription factor MYC.[19–24] Omomyc forms homodimers that bind to the MYC recognition sequence (E-box) and competitively inhibit MYC's oncogenic transcriptional activity. It offers several advantages as a model system for evaluating intracellular protein delivery strategies. First, Omomyc is biophysically well

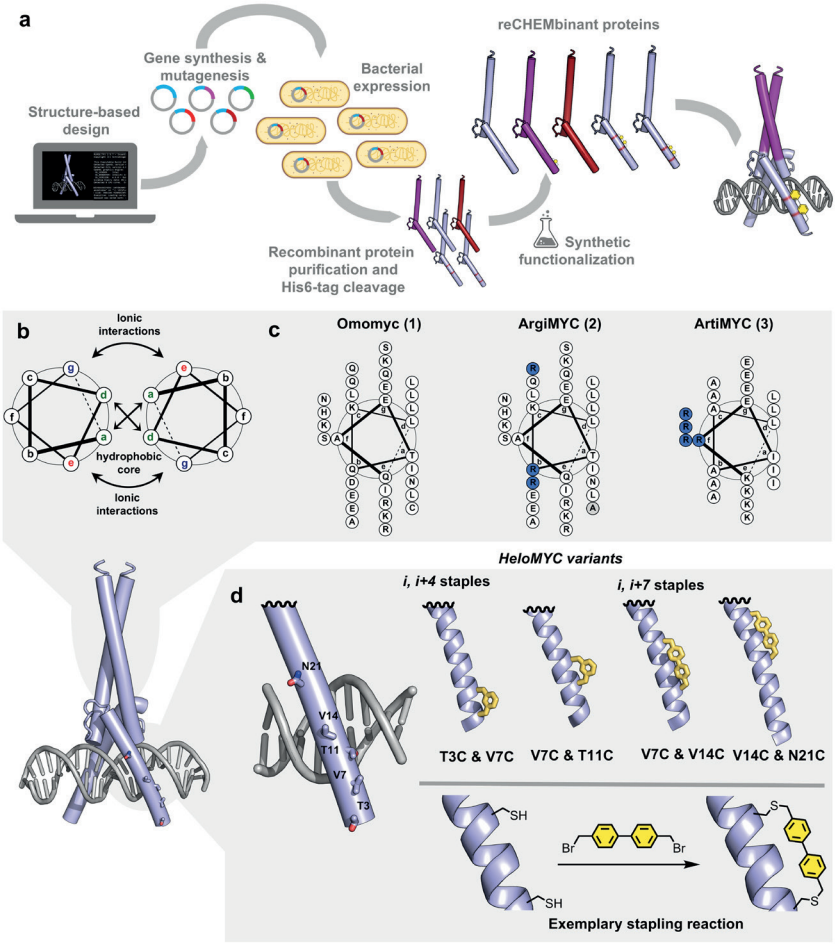

▲**Figure 4.1 ReCHEMbinant protein design.** (**a**) Design, generation and synthetic modification of reCHEMbinant proteins. After structure evaluation and mutagenesis his-tagged proteins are expressed in E. coli cells. The his-tag is then cleaved and, if applicable, the purified proteins are reacted with a staple. (**b**) Helical wheel showing heptad pattern and the interactions between the α-helices in a coiled-coil. (**c**) Helical wheel representation of the coiled-coil helices of Omomyc (**1**), ArgiMYC (**2**) and ArtiMYC (**3**). (**d**) DNA-binding basic part of Omomyc with residues highlighted that have been identified for mutation and stapling. Two residues are mutated into Cys and reacted with a staple.

understood, and quantitative assays such as DNA-binding electrophoretic mobility shift assays (EMSAs) enable precise evaluation of structural and functional integrity following chemical modification. Second, functional cellular readouts, including luciferase-based MYC reporter assays, provide rapid assessment of intracellular delivery and bioactivity. Third, Omomyc is recombinantly expressed in bacteria and

is of moderate size, facilitating high-resolution analytical characterization such as intact protein mass spectrometry. Notably, Omomyc exhibits some intrinsic cell-penetrating activity;[25] however, conflicting reports suggest that its native uptake is limited and insufficient for robust therapeutic effects.[11] These combined features, biochemical tractability, functional relevance, and borderline permeability, make Omomyc an ideal system for testing and optimizing chemically enhanced intracellular delivery strategies with potential therapeutic impact

Here, we developed a reCHEMbinant protein engineering strategy that combines structure-guided design and recombinant expression of Omomyc analogs with targeted chemical modification. By introducing a series of sequence-based mutations and covalent stabilization elements, we generated stapled Omomyc variants with enhanced physicochemical and functional properties. This approach led to the identification of a reCHEMbinant class of compounds capable of efficient cellular uptake and potent inhibition of MYC-driven transcription. Our lead construct, HeloMYC-1421, exhibits low-nanomolar DNA-binding affinity and submicromolar potency in a MYC reporter assay, substantially outperforming unmodified Omomyc. Fluorescence imaging confirmed markedly improved cellular penetration, and further characterization demonstrated selective anti-proliferative effects in MYC-dependent cancer cells, with no observable toxicity in MYC-independent lines. These findings establish reCHEMbinant stapling as a promising strategy for enabling intracellular delivery and therapeutic modulation of recombinant protein biologics.

4.2 Results

4.2.1 Design and synthesis of reCHEMbinant transcription factors

To engineer protein variants with high affinity for E-Box DNA and improved bioactivity, particularly with a focus on cell penetration, we used Omomyc as a template. Our approach involved preserving its overall structural and functional characteristics while introducing targeted mutations to optimize bioactivity. We pursued two key strategies: (1) incorporating canonical sequence mutations to increase arginine content, and (2) introducing chemical modifications aimed at enhancing structural stability and promoting cell penetration.

The cell penetrating properties of polycationic arginine rich peptides have been extensively reported.[26] Studies about Omomyc's intrinsic cell penetrating properties have revealed that the arginines in the DNA binding helix are critical for this ability. [25] However, an excessive arginine content is associated with non-specific toxicity.[27–29] In an attempt to balance potential cell penetrating efficacy and safety, we decided to modify the coiled-coil region of Omomyc, matching its arginine content to that of its DNA-binding helix. We first selected solvent exposed residues, which based on structural analysis, are not involved in the protein dimerization and generated

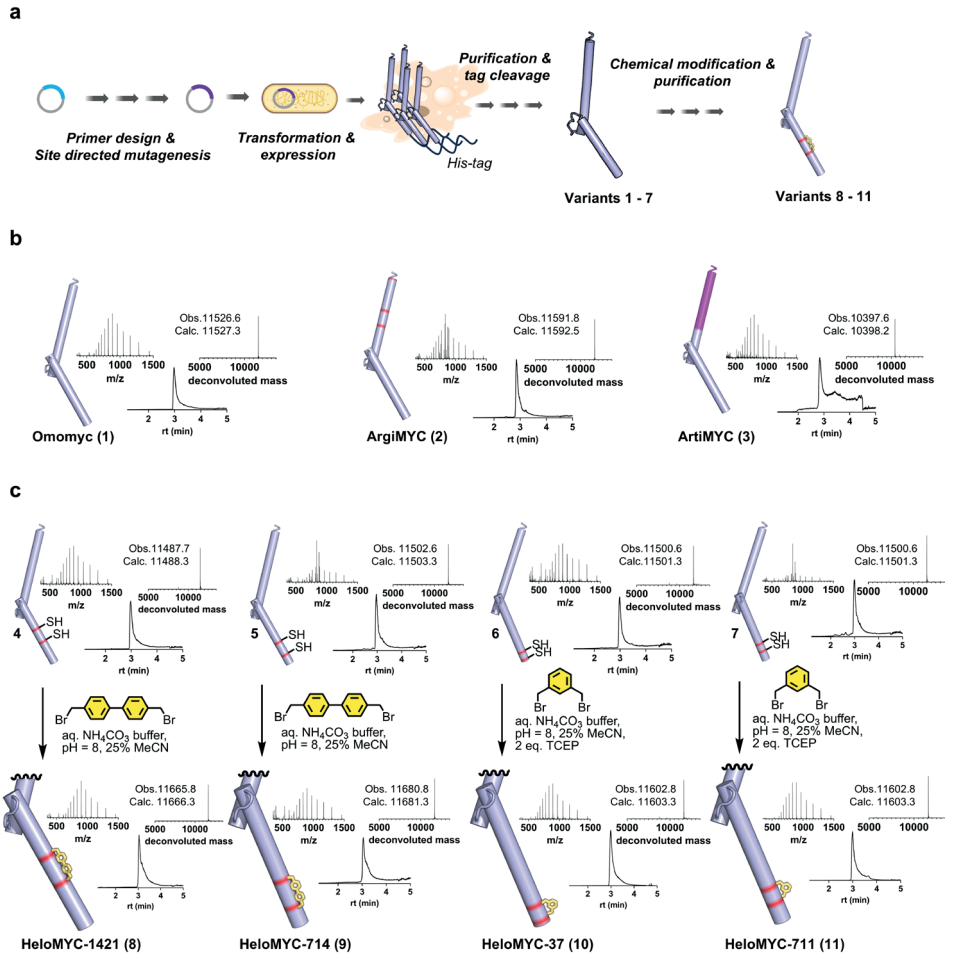

▲**Figure 4.2 Generation of artificial transcription factors.** (**a**) General workflow for generation of HeloMYC synthetic transcription factors by recombinant expression and chemical modification. (**b**) Omomyc (**1**, left) and coiled-coil modified Omomyc variants ArgiMYC (**2**) and ArtiMYC (**3**) were obtained by recombinant expression in good purity. **(c**) Point-mutated Omomyc derivatives obtained by recombinant expression in excellent purity (upper part) were reacted with the desired staple to generate the different HeloMYC proteins **8**-**11**.

a variant, ArgiMYC, in which we mutated three residues (Q64, D71, and Q86) to arginine (**Figure 4.1c**, middle). In a second approach, we designed a fully artificial coiled coil (residues 61-83), also with increased arginine content compared to the wild-type protein (**Figure 4.1c**, right). The predicted AlphaFold structure of the resulting ArtiMYC dimer aligned well with wild-type Omomyc (**Figure S4.1**). ArgiMYC and ArtiMYC possess an overall slightly increased arginine content of 11.1% and 13.3%, respectively, compared to Omomyc with 9.7%.

To chemically enhance the protein variants, we employed a semisynthetic strategy we refer to as the *reCHEMbinant* approach. Chemical staples, which stabilize the α-helical conformation of peptides, have been shown to improve cell penetration, stability, and overall bioactivity.[30–32] These staples are covalent linkages between amino acid side chains spaced one or two helix turns apart (*i, i+4* or *i, i+7*, respectively). The enhanced cell penetration of stapled helices is attributed to increased lipophilicity from the staple and the locked α-helical structure, which engages all backbone amides in intramolecular hydrogen bonding.[31] In our *reCHEMbinant* approach, we adhered to the following steps: (1) identify suitable *i, i+4* and *i, i+7* positions based on structural analysis, (2) mutate the selected residues pairwise to cysteines, (3) recombinantly express and purify the proteins, and (4) staple the proteins using cysteine-reactive bifunctional reagents (**Figure 4.1a**).[33,34] We selected four pairwise mutations, two for *i, i+4* and two for *i, i+7* stapling, modifying the backside of the DNA-binding helix to avoid disrupting DNA recognition (**Figure 4.1d**).

We prepared all plasmids with the desired mutations and expressed the proteins in ArcticXpress cells. We purified via Ni-NTA affinity chromatography and subsequently cleaved the tags releasing the pure protein products. Omomyc (1), ArgiMYC (2) and ArtiMYC (3) were all obtained in satisfying yield (8-14 mg/L culture) and purity, as shown by LC-MS (**Figure 4.2a-b**). These three variants (1, 2 and 3) were not further synthetically modified. We also expressed and purified the bis-cysteine variants and further modified the proteins with either 4,4'-bis(bromomethyl)-1,1'-biphenyl or 1,3-bis(bromomethyl)benzene. The *i, i + 4* cysteine pairs required addition of reducing agent (TCEP) during the reaction, to prevent disulfide formation. All site specific protein functionalizations resulted in clean conversions and we obtained the four reCHEMbinant stapled proteins, HeloMYC-37, -711, -714 and -1421 (**Figure 4.2c)**.

4.2.2 Biophysical characterization and binding evaluation

We measured the affinity to E-Box DNA of all reCHEMbinant transcription factors using EMSA. Based on their design, all our engineered protein variants are supposed to homodimerize, bind to E-Box DNA and result in a detectable shift when measured via native gel electrophoresis. To visualize the DNA and the protein-DNA complexes we incubated all variants with 5'-IRD700-labelled dsDNA containing the E-Box sequence CACGTG and resolved the mixture on a native gel. We then quantified the bound fraction of DNA and calculated K_D values. The control protein Omomyc binds DNA with a K_D of 22 nM. ArgiMYC (**2**) showed a K_D of 100 nM, but consistently resulted in smeared bands, potentially indicating partial unspecific binding. ArtiMYC (**3**) binds E-Box with 24 nM, an affinity comparable to Omomyc. The HeloMYC variants resulted in K_D values between 15 and 8 nM, which represents a 2-3 fold improvement in affinity compared to their unmodified parent compound Omomyc (**Figure 4.3a-c**).

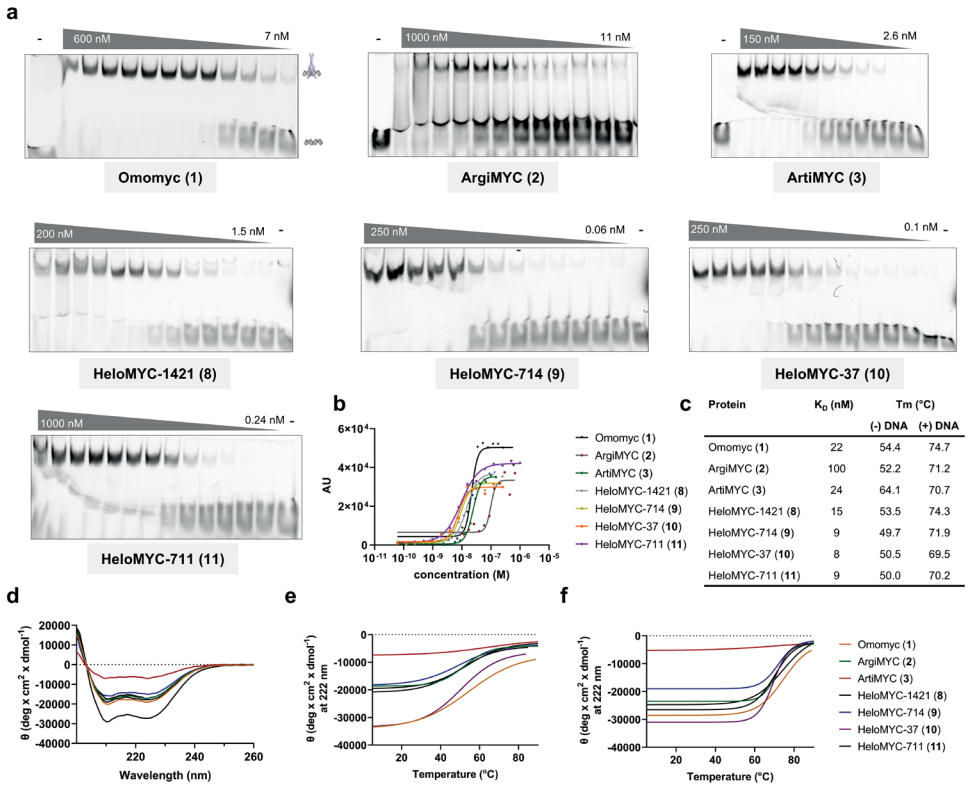

Protein	K_D (nM)	Tm (°C)	
		(-) DNA	(+) DNA
Omomyc (**1**)	22	54.4	74.7
ArgiMYC (**2**)	100	52.2	71.2
ArtiMYC (**3**)	24	64.1	70.7
HeloMYC-1421 (**8**)	15	53.5	74.3
HeloMYC-714 (**9**)	9	49.7	71.9
HeloMYC-37 (**10**)	8	50.5	69.5
HeloMYC-711 (**11**)	9	50.0	70.2

▲Figure 4.3 ReChembinant transcription factors bind to E-Box DNA with high potency. (**a**) EMSAs of ReChembinant transcription factors with 5'-IRD700-labelled dsDNA (sequence 5′-IRD700-ACCCCAC**CACGTG**GTGCCT–3′) show DNA binding of Omomyc (**1**), ArgiMYC (**2**), ArtiMYC (**3**) and HeloMYC variants (**8-11**). DNA construct is incubated with miniprotein and the mixture resolved by native gel electrophoresis. DNA binding is seen as the DNA-protein complex running higher than free DNA. (**b**) Plot of curves used for K_D-value determination. AU values were obtained by quantifying the signal of the bound fraction of DNA. (**c**) Summary of all K_D-values as determined by EMSA and structural melting points as determined by CD in absence and presence of E-Box DNA. (**d**) CD spectra of all constructs. (**e-f**) CD melting curves of all constructs in absence (**e**) and presence (**f**) of E-Box DNA, measured at 222 nm.

We used circular dichroism (CD) to evaluate structural features and structural stability of all variants. CD spectra of all proteins exhibit defined minima at around 208 nm and 222 nm indicating α-helical folding (**Figure 4.3d**). Only ArtiMYC (**3**) showed a weaker CD signal, albeit still indicating alpha helicity. This effect might result from aggregation but we did not investigate further this phenomenon. We also performed CD melting experiments in absence and presence of DNA. In all cases the presence of DNA resulted in significant structural stabilization (approximately +20 °C), further confirming the functional DNA binding of these variants.

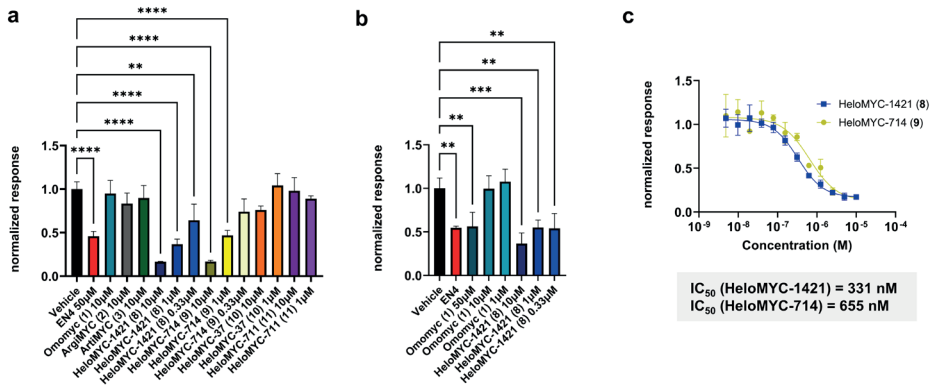

▲Figure 4.4 Biphenyl-stapled HeloMYC miniproteins significantly reduce MYC-related gene transcription in a reporter assay. (**a,b**) HEK293T (**a**) and HeLa (**b**) cells transiently transfected with a MYC-dependent luciferase gene were incubated with transcriptional repressor miniproteins or small molecule MYC inhibitor EN4 for one day and luciferase activity measured subsequently. HeloMYC-714 and HeloMYC-1421 show significant downregulation of MYC-related luciferase expression. (**c**) IC_{50} values for MYC-regulated luciferase expression inhibition by HeloMYC-1421 and HeloMYC-714 were measured in transiently transfected HEK293T cells. **Statistics.** A one way ANOVA was performed to compare the effect of miniprotein treatment on normalized signal showing that there was a statistical difference between treatments. (a) $F(14, 30) = 22.76$, $P<0.0001$; (b) $F(7, 16) = 13.21$, $P<0.0001$. * $p<0.05$, ** $p<0.01$, *** $p<0.001$.

Taken together, our set of biophysical assays indicate robust DNA binding activity and alpha helical folding for the four stapled HeloMYC variants (**8-11**). ArgiMYC and ArtiMYC showed less convincing results in the EMSA assay and CD analysis, respectively.

4.2.3 Evaluation of bioactivity

To evaluate the intracellular effects of our reCHEMbinant protein variants, we performed MYC-responsive reporter gene assays, which revealed that only the *i,i*+7-stapled constructs HeloMYC-714 and HeloMYC-1421 elicited significant cellular activity. These assays use a firefly luciferase gene activated by MYC/MAX dimers, with a constitutively expressed renilla luciferase under control of the CMV promoter for normalization. Following transfection of HEK293T with dual reporter DNA, cells were treated for 24 hours with Omomyc or our mutated reCHEMbinant transcription factors. We also included the small molecule covalent MYC inhibitor EN4 as a positive control.[35] Based on previous reports the main expected mechanism of action of Omomyc and analogs would be forming dimers and occupying the MYC/MAX DNA binding sites.[25] Among all protein variants only the *i, i+7*-stapled

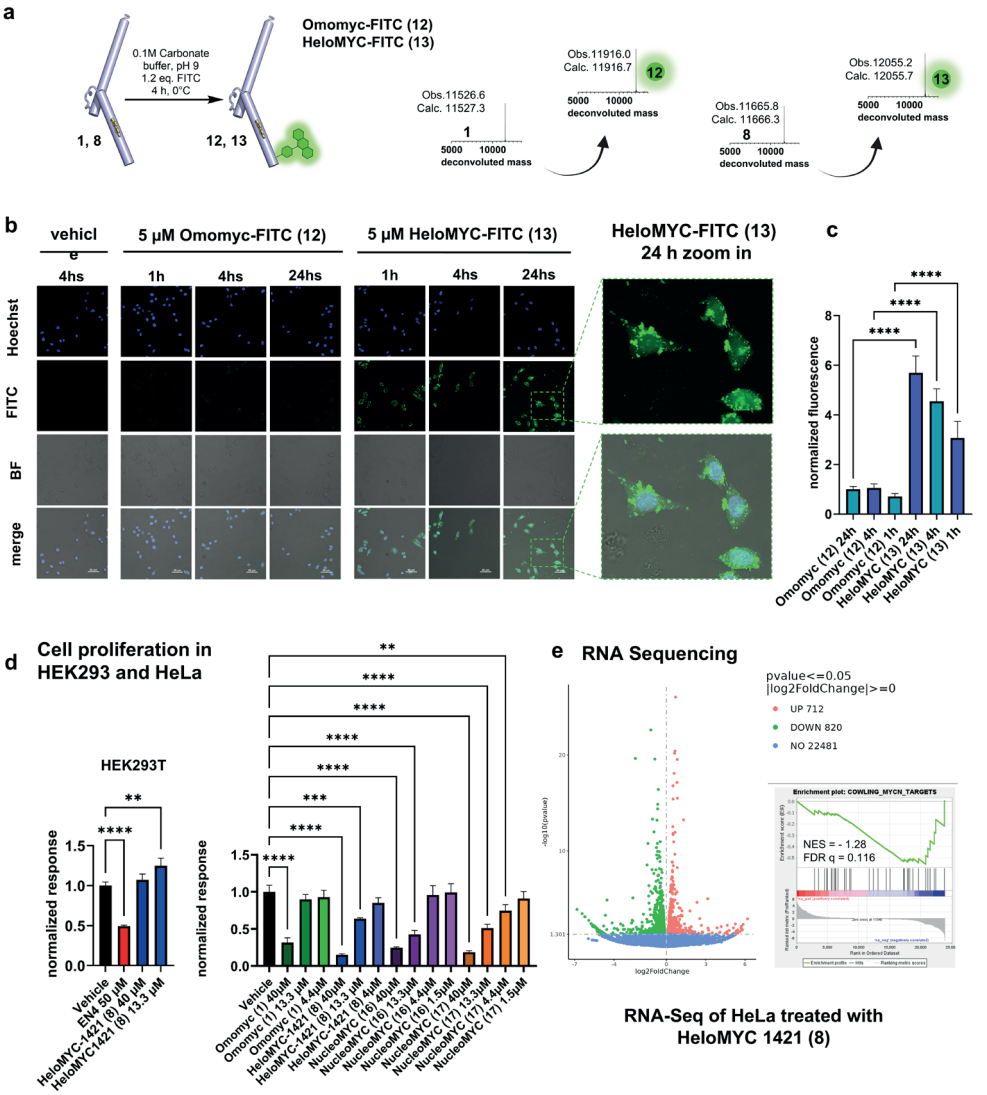

proteins HeloMYC-714 and -1421 displayed a significant downregulation of MYC reporter activity (**Figure 4.4a**). Both HeloMYC derivatives exhibit roughly the same effect on MYC activity at 1 µM concentration as EN4 does at 50 µM. We then went on to measure their EC_{50} values in the reporter gene assay which we determined to be 655 nM for HeloMYC-714 and 331 nM for HeloMYC-1421 (**Figure 4.4c**, data from 3 independent experiments in **Figure S4.2**). To corroborate these findings, we tested a subset of compounds (HeloMYC-1421 (**8**), Omomyc (**1**), and EN4) in HeLa cells, where HeloMYC-1421 (**8**) again showed potent reporter downregulation at sub-micromolar concentrations, whereas Omomyc (**1**) was only effective at 50 µM (**Figure 4.4b**). In our control experiments we confirmed that the constructs had

◀Figure 4.5 HeloMYC-1421 is cell permeable and inhibits cell proliferation of cancer cell lines. **(a)** Omomyc (**1**) and HeloMYC-1421 (**8**) were reacted with FITC in carbonate buffer. **(b)** Fluorescence microscopy of live HeLa cells treated with HeloMYC-FITC (**13**) or Omomyc-FITC (**12**), imaged at 1 h, 4 h and 24 h. **(c)** Quantification of fluorescence shows superior cell permeability of HeloMYC-FITC (**13**) (**d**) Cell titer glow (CTG) assays to assess HeloMYC-1421 (**8**) activity proliferation of HEK293T and CTG assay in HeLa cells with HeloMYC-1421 (**8**) and NucleoMYC **16** and **17**. e) HeLa cells were treated with HeloMYC-1421 (**8**) at 10 **μ**M for 3 days. RNA was extracted and sequenced. Shown are up- (rosa) and down- (green) regulated genes with p value < 0.05 and on the right the GSEA plot for the COWLING_MYC_Targets is shown. **Statistics.** A one way ANOVA was performed to compare the effect of miniprotein treatment on normalized signal showing that there was a statistical difference between treatments. (b) $F(5, 186) = 132.8$, $P<0.0001$; (d) HEK293T $F(3, 8) = 75.49$, $P<0.0001$; HeLa $F(14, 28) = 49.17$, $P<0.0001$. * $p<0.05$, ** $p<0.01$, *** $p<0.001$.

no impact on the constitutively expressed CMV-driven renilla luciferase, but that HeloMYC-1421 and EN4 exhibited a negative effect on constitutively expressed CMV driven firefly luciferase. We could experimentally exclude that these compounds act as direct enzymatic inhibitors, by adding the constructs to control-transfected cells directly before cell lysis and luciferase read-out. These experiments therefore, in addition to direct MYC inhibition, hint at a likely more complex inhibition pathway mechanism (**Figure S4.3** for validation data). Despite this uncertainty, the MYC reporter gene assays indicated strong intracellular activity for the *i, i+7* biphenyl-stapled proteins HeloMYC-714 and HeloMYC-1421, while all other variants, including Omomyc, showed little to no effects.

To investigate whether the improved activity of the HeloMYC variants in the reporter gene assay is a result of improved cell penetration we turned to fluorescence microscopy. Given that the protein variants **2** and **3** with increased arginine content and the variants with the *i, i* + 4 staples had not shown any cell activity, we only proceeded with analyzing HeloMYC-1421 and comparing it to the unmodified parent protein Omomyc.

Fluorescence imaging revealed that HeloMYC-1421 enters cells more efficiently than Omomyc. We labeled HeloMYC-1421 and Omomyc with fluorescein isothiocyanate (FITC) and purified the resulting variants **12** and **13** (**Figure 4.5a**). We then performed live cells imaging in HeLa cells upon incubation with the fluorescent proteins (at 5 μM) for either 1 h, 4 h or 24 h. At all timepoints HeloMYC-FITC (**13**) is taken up into cells significantly more than Omomyc-FITC (**12**). We observed that the uptake increases over time and also enhanced colocalization with the nucleus (**Figure 4.5c**). This time course points toward an endocytosis bases cell entry mechanism followed by partial endosomal escape. **Figure 4.5b** shows that part of the compound remains localized in endosomal structures (green puncta), while a substantial fraction is also diffusely distributed throughout the cytosol and nucleus. The more efficient cell penetration compared to Omomyc can likely explain the enhanced efficacy of the

HeloMYC variants in the reporter gene assay.

As alpha helix stapling is often associated with improved resistance against proteases, we also performed a serum stability assay to compare unmodified Omomyc (1) to HeloMYC-1421 (**8**). We incubated both proteins in 10% human serum and assessed their half lives by LCMS (**Figure S4.4**). HeloMYC-1421 (**8**) displayed a significant improved stability compared to Omomyc (4.8 h compared to 1.3 h). In addition to the better cell uptake, also the stability can be part of the explanation of the improved bioactivity.

HeloMYC-1421 (**8**) inhibits the proliferation of cancer cells without inducing nonspecific cytotoxicity in MYC-independent cells. To assess potential off-target toxicity, we treated HEK293T cells—which do not rely on MYC for survival—with HeloMYC-1421 (**8**). The cells tolerated treatment well, showing no loss of viability after 3 days at concentrations up to 40 μM (**Figure 4.5d**). In contrast, MYC-dependent HeLa cells showed a significant reduction in proliferation at concentrations as low as 13.3 μM. To enhance nuclear delivery, we generated HeloMYC-1421 variants bearing nuclear localization sequences (NLS) at either the N- or C-terminus (NucleoMYC **16** and **17**, **Figure S4.5**). NucleoMYC **17** showed a modest improvement in potency, although overall the NLS addition had only a moderate effect. Collectively, these data show that HeloMYC-1421 and its NLS-tagged variants inhibit cancer cell proliferation at 13.3 μM (compounds **8** and **16**) and 4.4 μM (compound **17**) and, importantly, the reCHEMbinant HeloMYC did not exhibit cytotoxicity in MYC-independent HEK293T cells.

HeloMYC-1421 (8) modulates MYC activity in HeLa cells, leading to significant transcriptional changes. After 3 days of treatment, RNA-seq analysis revealed 712 upregulated and 820 downregulated genes. Gene Set Enrichment Analysis (GSEA) uncovered a trend toward coordinated downregulation of the Cowling MYC target gene set, reflecting partial suppression of MYC-driven transcription. Although the enrichment was modest, this subtle effect aligns with the expected mechanism of the inhibitor, which tempers MYC function rather than fully abolishing it, unlike the complete loss seen in knockout models used for the gene set comparisons. This nuanced modulation supports the therapeutic potential of HeloMYC-1421.

As a final experiment, we explored whether the stapling position in reCHEMbinant transcription factors could also serve as a site for the conjugation of additional functional groups, such as small molecules or affinity handles. To this end, we designed and synthesized two trifunctional probes containing a dibromomaleimide moiety for stapling via two cysteines, with an additional functionality introduced through substitution at the maleimide nitrogen. Probe 18 carried a biotin handle, while probe 19 contained the BET inhibitor JQ1, a compound known to modulate MYC expression. HeloMYC-711 (11) was reacted with these probes in aqueous

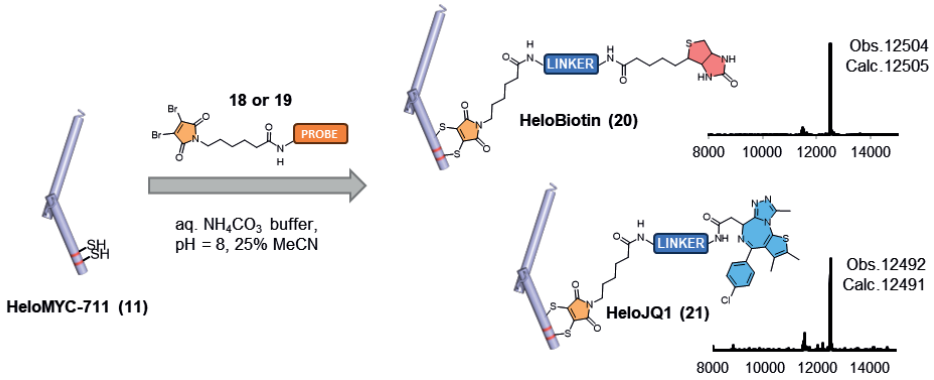

▲**Figure 6. Synthesis of reCHEMbinant protein conjugates.** The reaction between HeloMYC-711 (11) and trifuctional dibromomaleimide-biotin (18) or dibromomaleimide-JQ1 (19) resulted in efficient conversion to HeloBiotin (20) and HeloJQ1 (21).

buffer, resulting in efficient conversion to the corresponding conjugates, HeloBiotin and HeloJQ1 (**Figure 4.6**). Although we did not pursue a detailed characterization of these conjugates, the straightforward synthetic strategy demonstrates a feasible route to generate chemically diversified protein variants that may be of use in future biochemical studies or for probing functional effects.

4.3 Discussion and conclusions

In this study, we developed a chemically enhanced protein engineering strategy targeting the nuclear DNA binding site of the oncogenic transcription factor MYC. Efficient intracellular delivery of proteins remains a key challenge for protein therapeutics.[9,10,12,13,36] Starting from Omomyc, a known MYC inhibitor with some intrinsic cell-penetrating properties, we explored two distinct strategies to improve cell permeability and bioactivity: (1) increasing the arginine content, inspired by polycationic cell-penetrating peptides, and (2) chemically modifying the DNA-binding domains with peptide staples.

While the arginine-rich variants, ArgiMYC and ArtiMYC and the *i, i* + 4 staples showed no detectable improvements in cell activity, the *i, i* + 7 stapled proteins, HeloMYC-714 and HeloMYC-1421, exhibited significantly enhanced cellular activity. Via fluorescent microscopy we confirmed that the biphenyl staple leads to a substantially improved uptake in cells. Interestingly, despite minimal impact on helical stability, the *i, i* + 7 stapling led to pronounced gains in cellular uptake, potentially due to the amphipathic nature of these constructs. The *i, i* + 4 xylene staple might not add enough hydrophobicity to the helix backside to achieve the same effect. Also, just slightly increasing the arginine content, as attempted in ArgiMYC and ArtiMYC, did

not lead to the desired enhanced cellular uptake. Three more arginines distributed along such a long sequence might not be enough for such activity. While arginine rich peptide often are cell penetrating, the arginine residues might require closer clustering as opposed to the distributed placement in ArgiMYC and ArtiMYC.

Our finding highlight the unique potential of protein stapling for generating cell-penetrant protein drugs targeting intracellular complexes. While peptide staples have been used to stabilize α-helical structures, protect against proteolytic degradation and improve cell permeability, [31,32,37] applying stapling techniques to entire recombinant proteins, aiming at these properties, to date remains largely underexplored. Protein stapling has been reported, but mainly in proof of principle studies or mainly aiming at tertiary structure stabilization.[38–41] While there have been previous efforts toward the chemical synthesis of MYC analogs,[16,17,24,42–48] we developed a practical reCHEMbinant workflow, for directly modifying recombinant proteins. Our reCHEMbinant approach, which combines recombinant protein expression with targeted cysteine modification, enables rapid generation of stapled protein variants and may be applicable to other α-helical protein domains. Recent technology breakthroughs enable the de novo design of miniproteins binding to virtually any target.[49] For intracellular targets these approaches are of limited interest, but our reCHEMbinant strategy could unlock this potential.

Our cell proliferation experiments showed how HeloMYC's ability to inhibit the proliferation of cancer cells, without showing toxicity on MYC-independent HEK293 cells, indicating the absence of unspecific membrane toxicity, sometimes observed for cell penetrating peptides.[29] While our HeloMYC variants showed a clear superiority to the parent compound Omomyc, their current potency in inhibiting cell proliferation suggests that further optimization will be necessary to fully realize their clinical potential. Overall, our findings demonstrate that this approach can significantly enhance the therapeutic potential of protein drugs, expanding their applicability to previously undruggable intracellular targets.

4.4 Contribution to the chapter

In this chapter we performed a structure-based design study using the crystal structure of Omomyc. We regularly discussed results (daily to weekly basis) and I provided advice where possible. I helped regularly with protein expression and performed stability and folding assays for the compounds described within this chapter. The latter entails the development of the serum stability assay and characterization of all compounds using CD. The staple reaction protocol was based on a protocol developed by me for **Chapter 3.** I helped with revisions.

4.5 References

[1] B. Leader, Q. J. Baca, D. E. Golan, "Protein therapeutics: a summary and pharmacological classification" *Nature Reviews Drug Discovery 2007 7:1* **2008**, *7*, 21–39.

[2] K. Itakura, T. Hirose, R. Crea, A. D. Riggs, H. L. Heyneker, F. Bolivar, H. W. Boyer, "Expression in Escherichia coli of a Chemically Synthesized Gene for the Hormone Somatostatin" *Science (1979)* **1977**, *198*, 1056–1063.

[3] M. M. Goldenberg, "Trastuzumab, a recombinant DNA-derived humanized monoclonal antibody, a novel agent for the treatment of metastatic breast cancer" *Clin Ther* **1999**, *21*, 309–318.

[4] G. Kwok, T. C. C. Yau, J. W. Chiu, E. Tse, Y. L. Kwong, "Pembrolizumab (Keytruda)" *Hum Vaccin Immunother* **2016**, *12*, 2777–2789.

[5] H. F. Bunn, "Erythropoietin" *Cold Spring Harb Perspect Med* **2013**, *3*, a011619.

[6] S. Pestka, "The Interferons: 50 Years after Their Discovery, There Is Much More to Learn" *Journal of Biological Chemistry* **2007**, *282*, 20047–20051.

[7] M. Buyanova, D. Pei, **2022**, Elsevier Ltd preprint, DOI: 10.1016/j.tips.2021.11.008.

[8] F. Cozzolino, I. Iacobucci, V. Monaco, M. Monti, **2021**, American Chemical Society preprint, DOI: 10.1021/acs.jproteome.1c00074.

[9] H. D. Herce, D. Schumacher, A. F. L. Schneider, A. K. Ludwig, F. A. Mann, M. Fillies, M. A. Kasper, S. Reinke, E. Krause, H. Leonhardt, M. C. Cardoso, C. P. R. Hackenberger, "Cell-permeable nanobodies for targeted immunolabelling and antigen manipulation in living cells" *Nat Chem* **2017**, *9*, 762–771.

[10] S. Mandal, G. Mann, G. Satish, A. Brik, "Enhanced Live-Cell Delivery of Synthetic Proteins Assisted by Cell-Penetrating Peptides Fused to DABCYL" *Angewandte Chemie - International Edition* **2021**, *60*, 7333–7343.

[11] E. Wang, A. Sorolla, P. T. Cunningham, H. M. Bogdawa, S. Beck, E. Golden, R. E. Dewhurst, L. Florez, M. N. Cruickshank, K. Hoffmann, R. M. Hopkins, J. Kim, A. J. Woo, P. M. Watt, P. Blancafort, "Tumor penetrating peptides inhibiting MYC as a potent targeted therapeutic strategy for triple-negative breast cancers" *Oncogene* **2019**, *38*, 140–150.

[12] K. A. Mix, J. E. Lomax, R. T. Raines, "Cytosolic Delivery of Proteins by Bioreversible Esterification" *J Am Chem Soc* **2017**, *139*, 14396–14398.

[13] J. V. Jun, Y. D. Petri, L. W. Erickson, R. T. Raines, "Modular Diazo Compound for the Bioreversible Late-Stage Modification of Proteins" *J Am Chem Soc* **2023**, *145*, 6615–6621.

[14] M. Wendt, R. Bellavita, A. Gerber, N. L. Efrém, T. van Ramshorst, N. M. Pearce, P. R. J. Davey, I. Everard, M. Vazquez-Chantada, E. Chiarparin, P. Grieco, S. Hennig, T. N. Grossmann, "Bicyclic β-Sheet Mimetics that Target the Transcriptional Coactivator β-Catenin and Inhibit Wnt Signaling" *Angewandte Chemie - International Edition* **2021**, *60*, 13937–13944.

[15] H. Adihou, R. Gopalakrishnan, T. Förster, S. M. Guéret, R. Gasper, S. Geschwindner, C. Carrillo García, H. Karatas, A. V Pobbati, M. Vazquez-Chantada, P. Davey, C. M. Wassvik, J. K. S. Pang, B. S. Soh, W. Hong, E. Chiarparin, D. Schade, A. T. Plowright, E. Valeur, M. Lemurell, T. N. Grossmann, H. Waldmann, "A protein tertiary structure mimetic modulator of the Hippo signalling pathway" *Nat Commun* **2020**, *11*, DOI 10.1038/s41467-020-19224-8.

[16] T. E. Speltz, Z. Qiao, C. S. Swenson, X. Shangguan, J. S. Coukos, C. W. Lee, D. M. Thomas, J. Santana, S. W. Fanning, G. L. Greene, R. E. Moellering, "Targeting MYC with modular synthetic transcriptional repressors derived from bHLH DNA-binding domains" *Nat Biotechnol* **2023**, *41*, DOI 10.1038/s41587-022-01504-x.

[17] B. D. Ellenbroek, J. P. Kahler, D. Arella, C. Lin, W. Jespers, E. A. Züger, M. Drukker, S. J. Pomplun, "Development of DuoMYC: a synthetic cell penetrant miniprotein that efficiently inhibits the oncogenic transcription factor MYC" *Angewandte Chemie International Edition* **2024**, DOI 10.1002/anie.202416082.

[18] M. Pelay-Gimeno, A. Glas, O. Koch, T. N. Grossmann, "Structure-Based Design of Inhibitors of Protein-Protein Interactions: Mimicking Peptide Binding Epitopes" *Angewandte Chemie International Edition* **2015**, *54*, 8896–8927.

[19] L. Soucek, R. Jucker, L. Panacchia, R. Ricordy, F. Tatò, S. Nasi, "Omomyc, a potential Myc dominant negative, enhances Myc-induced apoptosis" *Cancer Res* **2002**, *62*, 3507–3510.

[20] M. J. Demma, C. Mapelli, A. Sun, S. Bodea, B. Ruprecht, S. Javaid, D. Wiswell, E. Muise, S. Chen, J. Zelina, F. Orvieto, A. Santoprete, S. Altezza, F. Tucci, E. Escandon, B. Hall, K. Ray, A. Walji, J. O'Neil, "Omomyc Reveals New Mechanisms To Inhibit the MYC Oncogene" *Mol Cell Biol* **2019**, *39*, 1–27.

[21] D. Massó-Vallés, L. Soucek, "Blocking Myc to Treat Cancer: Reflecting on Two Decades of Omomyc" *Cells* **2020**, *9*, 883.

[22] L. A. Jung, A. Gebhardt, W. Koelmel, C. P. Ade, S. Walz, J. Kuper, B. Von Eyss, S. Letschert, C. Redel, L. D'Artista, A. Biankin, L. Zender, M. Sauer, E. Wolf, G. Evan, C. Kisker, M. Eilers, "OmoMYC blunts promoter invasion by oncogenic MYC to inhibit gene expression characteristic of MYC-dependent tumors" *Oncogene* **2017**, *36*, 1911–1924.

[23] S. Pomplun, M. Jbara, C. K. Schissel, S. Wilson Hawken, A. Boija, C. Li, I. Klein, B. L. Pentelute, "Parallel Automated Flow Synthesis of Covalent Protein Complexes That Can Inhibit MYC-Driven Transcription" *ACS Cent Sci* **2021**, *7*, 1408–1418.

[24] M. Jbara, S. Pomplun, C. K. Schissel, S. W. Hawken, A. Boija, I. Klein, J. Rodriguez, S. L. Buchwald, B. L. Pentelute, "Engineering Bioactive Dimeric Transcription Factor Analogs via Palladium Rebound Reagents" *J Am Chem Soc* **2021**, *143*, 11788–11798.

[25] M. E. Beaulieu, T. Jauset, D. Massó-Vallés, S. Martínez-Martín, P. Rahl, L. Maltais, M. F. Zacarias-Fluck, S. Casacuberta-Serra, E. S. Del Pozo, C. Fiore, L. Foradada, V. C. Cano, M. Sánchez-Hervás, M. Guenther, E. R. Sanz, M. Oteo, C. Tremblay, G. Martín, D. Letourneau, M. Montagne, M. Á. M. Alonso, J. R. Whitfield, P. Lavigne, L. Soucek, "Intrinsic cell-penetrating activity propels omomyc from proof of concept to viable anti-myc therapy" *Sci Transl Med* **2019**, *11*, 1–14.

[26] N. Schmidt, A. Mishra, G. H. Lai, G. C. L. Wong, **2010**, DOI: 10.1016/j.febslet.2009.11.046.

[27] G. Tünnemann, G. Ter-Avetisyan, R. M. Martin, M. Stöckl, A. Herrmann, M. C. Cardoso, "Live-cell analysis of cell penetration ability and toxicity of oligo-arginines" *Journal of Peptide Science* **2008**, *14*, 469–476.

[28] E. M. López-Vidal, C. K. Schissel, S. Mohapatra, K. Bellovoda, C. L. Wu, J. A. Wood, A. B. Malmberg, A. Loas, R. Gómez-Bombarelli, B. L. Pentelute, "Deep Learning Enables Discovery of a Short Nuclear Targeting Peptide for Efficient Delivery of Antisense Oligomers" *JACS Au* **2021**, *1*, 2009–2020.

[29] C. Schissel, S. Mohapatra, J. Wolfe, C. Fadzen, K. Bellovoda, C.-L. Wu, J. Wood, A. Malmberg, A. Loas, R. Gómez-Bombarelli, B. Pentelute, "Interpretable Deep Learning for De Novo Design of Cell-Penetrating Abiotic Polymers" **2020**, DOI 10.1101/2020.04.10.036566.

[30] Q. Chu, R. E. Moellering, G. J. Hilinski, Y. W. Kim, T. N. Grossmann, J. T. H. Yeh, G. L. Verdine, "Towards understanding cell penetration by stapled peptides" *Medchemcomm* **2015**, *6*, 111–119.

[31] A. Chandramohan, H. Josien, T. Y. Yuen, R. Duggal, D. Spiegelberg, L. Yan, Y. C. A. Juang, L. Ge, P. G. Aronica, H. Y. K. Kaan, Y. H. Lim, A. Peier, B. Sherborne, J. Hochman, S. Lin, K. Biswas, M. Nestor, C. S. Verma, D. P. Lane, T. K. Sawyer, R. Garbaccio, B. Henry, S. Kannan, C. J. Brown, C. W. Johannes, A. W. Partridge, "Design-rules for stapled peptides with in vivo activity and their application to Mdm2/X antagonists" *Nat Commun* **2024**, *15*, DOI 10.1038/s41467-023-43346-4.

[32] Y. W. Kim, T. N. Grossmann, G. L. Verdine, "Synthesis of all-hydrocarbon stapled ±-helical peptides by ring-closing olefin metathesis" *Nat Protoc* **2011**, *6*, 761–771.

[33] P. Timmerman, W. C. Puijk, R. H. Meloen, "Functional reconstruction and synthetic mimicry of a conformational epitope using CLIPS™ technology" *Journal of Molecular Recognition* **2007**, *20*, 283–299.

[34] S. S. Kale, C. Villequey, X. D. Kong, A. Zorzi, K. Deyle, C. Heinis, "Cyclization of peptides with two chemical bridges affords large scaffold diversities" *Nat Chem* **2018**, *10*, 715–723.

[35] L. Boike, A. G. Cioffi, F. C. Majewski, J. Co, N. J. Henning, M. D. Jones, G. Liu, J.

M. McKenna, J. A. Tallarico, M. Schirle, D. K. Nomura, "Discovery of a Functional Covalent Ligand Targeting an Intrinsically Disordered Cysteine within MYC" *Cell Chem Biol* **2021**, *28*, 4-13.e17.

[36] J. Liu, T. Gaj, M. C. Wallen, C. F. Barbas, "Improved cell-penetrating zinc-finger nuclease proteins for precision genome engineering" *Mol Ther Nucleic Acids* **2015**, *4*, e232.

[37] D. P. Fairlie, A. Dantas de Araujo, "Review stapling peptides using cysteine crosslinking" *Biopolymers* **2016**, *106*, 843–852.

[38] X. H. Chen, Z. Xiang, Y. S. Hu, V. K. Lacey, H. Cang, L. Wang, "Genetically encoding an electrophilic amino acid for protein stapling and covalent binding to native receptors" *ACS Chem Biol* **2014**, *9*, 1956–1961.

[39] S. P. Brown, A. B. Smith, "Peptide/protein stapling and unstapling: Introduction of s-tetrazine, photochemical release, and regeneration of the peptide/protein" *J Am Chem Soc* **2015**, *137*, 4034–4037.

[40] S. Neubacher, J. M. Saya, A. Amore, T. N. Grossmann, "In Situ Cyclization of Proteins (INCYPRO): Cross-Link Derivatization Modulates Protein Stability" *Journal of Organic Chemistry* **2020**, *85*, 1476–1483.

[41] G. H. Hutchins, S. Kiehstaller, P. Poc, A. H. Lewis, J. Oh, R. Sadighi, N. M. Pearce, M. Ibrahim, I. Drienovská, A. M. Rijs, S. Neubacher, S. Hennig, T. N. Grossmann, "Covalent bicyclization of protein complexes yields durable quaternary structures" *Chem* **2024**, *10*, 615–627.

[42] L. E. Canne, A. R. Ferré-D'Amaré, S. K. Burley, S. B. H. Kent, "Total Chemical Synthesis of a Unique Transcription Factor-Related Protein: cMyc—Max" *J Am Chem Soc* **1995**, *117*, 2998–3007.

[43] R. Calo-Lapido, C. Penas, A. Jiménez-Balsa, M. E. Vázquez, J. L. Mascareñas, "A chemical approach for the synthesis of the DNA-binding domain of the oncoprotein MYC" *Org Biomol Chem* **2019**, *17*, 6748–6752.

[44] B. D. Ellenbroek, J. P. Kahler, S. R. Evers, S. J. Pomplun, "Synthetic Peptides: Promising Modalities for the Targeting of Disease-Related Nucleic Acids" *Angewandte Chemie International Edition* **2024**, *63*

[45] O. Harel, M. Jbara, "Chemical Synthesis of Bioactive Proteins" *Angewandte Chemie - International Edition* **2023**, *62*, DOI 10.1002/anie.202217716.

[46] X. Lin, O. Harel, M. Jbara, "Chemical Engineering of Artificial Transcription Factors by Orthogonal Palladium(II)-Mediated S-Arylation Reactions" *Angewandte Chemie - International Edition* **2023**, *202317511*, DOI 10.1002/anie.202317511.

[47] R. V. Nithun, Y. M. Yao, X. Lin, S. Habiballah, A. Afek, M. Jbara, "Deciphering the Role of the Ser-Phosphorylation Pattern on the DNA-Binding Activity of Max Transcription Factor Using Chemical Protein Synthesis" *Angewandte Chemie - International Edition* **2023**, *62*, DOI 10.1002/anie.202310913.

[48] S. Pomplun, M. Jbara, C. K. Schissel, S. Wilson Hawken, A. Boija, C. Li, I. Klein, B. L. Pentelute, "Parallel Automated Flow Synthesis of Covalent Protein Complexes That Can Inhibit MYC-Driven Transcription" *ACS Cent Sci* **2021**, *7*, 1408–1418.

[49] M. Pacesa, L. Nickel, C. Schellhaas, J. Schmidt, E. Pyatova, L. Kissling, P. Barendse, J. Choudhury, S. Kapoor, A. Alcaraz-Serna, Y. Cho, K. H. Ghamary, L. Vinué, B. J. Yachnin, A. M. Wollacott, S. Buckley, A. H. Westphal, S. Lindhoud, S. Georgeon, C. A. Goverde, G. N. Hatzopoulos, P. Gönczy, Y. D. Muller, G. Schwank, D. C. Swarts, A. J. Vecchio, B. L. Schneider, S. Ovchinnikov, B. E. Correia, "One-shot design of functional protein binders with BindCraft" *Nature 2025* **2025**, 1–10.

4.6 Experimental

All reactions were carried out using commercially available reagents, unless noted otherwise. Reagents and solvents were purchased from Sigma-Aldrich (Merck), Fisher Scientific, or VWR chemicals.

Plasmid pET-30a with 6-his-tagged Omomyc was donated by the group of prof. dr. Eilers (University of Würzburg, Germany) and sequenced before being used. Primers for site-directed DNA mutagenesis were purchased from IDT (Leuven, Belgium). Plasmids with ArgiMYC, ArtiMYC and NucleoMYCs were obtained from genscript.

4.6.1 LC-MS

LC-MS chromatograms and associated mass spectra were acquired using a Shimazu LCMS-2020 system (Method A) or, for high resolution mass spectrometry data, a Sciex X500b QTOF ESI-QToF mass spectrometer coupled to a Shimadzu Nexera UHPLC LC40DX3 (Method B). Mobile phases used for LC-MS analysis are solvent A (0.1% formic acid in water) and solvent B (0.1% formic acid in acetonitrile).

The following LCMS methods were used:

Method A

Column: Kinetex® 2.6µm XB-C18 100 Å LC Column (50 x 3 mm) UV detector: 214 nm.

LC Method: 0% solvent B over 1 min, followed by a linear gradient 0% to 70% solvent B over 10 min, followed by 70% solvent B over 1.5 min, followed by 70% to 0% solvent B over 4.5, flowrate 0.55 mL/min

Method B (high resolution)

Column: Phenomenex Synergi™ 4 µm Fusion-RP 80 Å LC Column (50 x 2 mm)

LC Method: 0% solvent B over 1 min, followed by a linear gradient 0% to 60% solvent B over 3.5 min, followed by a linear gradient 60% to 95% solvent B over 0.1 min, followed by 95% solvent B over 0.4 min, followed by a linear gradient 95% to 0% solvent B over 0.5 min, followed by 0% solvent B over 1.5 min, flowrate 0.5 mL/min.

MS parameters: General parameters: Method duration: 5 min; Total scan time: 0.276 sec; Estimated cycles: 1086; Intact protein mode: False; Decrease detector voltage: False; Large protein (>70 kDa): False; Ion Source: Source name: TurbolonSpray; Curtain gas: 35 psi; Ion source gas 1: 60 psi; Ion source gas 2: 60 psi; Temperature: 500

˚C; Experiment: Scan type: TOF MS; Polarity: Positive; Spray voltage: 5500 V; CAD gas: 7; Time bins to sum: 4; Channel 1-4: True; TOF start mass: 350 Da; TOF stop mass 1500 Da; Accumulation time: 0.25; Declustering potential: 80V; Declustering potential spread: 0 V; Collision energy: 10V; Collision energy spread: 0 V; Override Qjet RF value: False

Method C (high resolution)

Column: Phenomenex Synergi™ 4 µm Fusion-RP 80 Å LC Column (50 x 2 mm) or Aeris™ 3.6 µm Widepore XB-C18.

LC Method: 0% solvent B over 1 min, followed by a linear gradient 0% to 90% solvent B over 6 min, followed by a 90% solvent B over 2 min, followed by a linear gradient of 90% to 0% solvent B over 0.5 min, followed by 0% solvent B over 1.5 min, flowrate 0.5 mL/min.

4.6.2 Synthesis

4.6.2.1 Stapling reactions

4.6.2.1.1 Stapling with i, i+7 staple (4,4′-Bis(bromomethyl)biphenyl)

The respective protein (1 eq., **4** or **5**) was dissolved in water (2 mM, e.g. 30 mg of **5** in 1.08mL) and then diluted to 100 µM into stapling buffer (15.12 mL for **5**, NH_4HCO_3, 100 mM, pH= 8). 4,4′-Bis(bromomethyl)biphenyl was dissolved at 4x the final concentration in MeCN (500 µM) and then added (1.25 eq., 5.4 mL for HeloMYC-1421) to the protein in stapling buffer. Final concentrations used were 100 µM (1 eq.) protein and 125 µM (1.25 eq.) staple. Final MeCN content was 25%.

When the stapling reaction was completed as seen by LC-MS the product was purified using a Biotage® Selekt Flash Purification System equipped with a Biotage® Sfär C18 D - Duo 10 g column on a gradient of water in MeCN (0-100%,with a flat gradient between 15% and 79%), both containing 0.1% TFA. The product containing fractions were lyophilized yielding the proteins as TFA salts.

Yield HeloMYC-1421 (**8**): 20.7 mg (69%)

Yield HeloMYC-714 (**9**): 1.94 mg (67%)

Yield NucleoMYC (**16**): 3.02 mg (60%)

Yield NucleoMYC (**17**): 3.71 mg (46%)

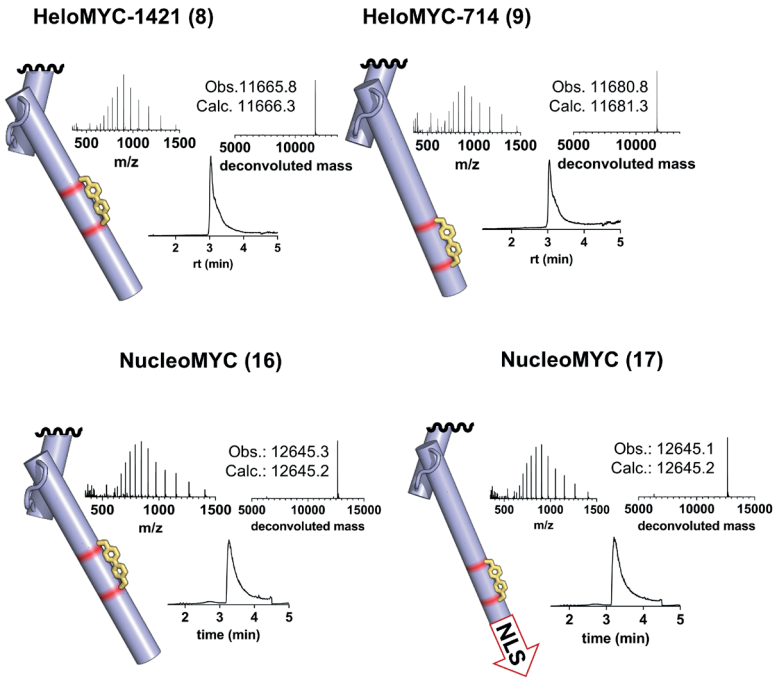

4

4.6.2.1.2 Stapling with i, i+4 staple (α,α-Dibromo-m-xylene)

The respective protein (1 eq., 6 or 7) was dissolved in water (2 mM, e.g. 1.96 mg of 7 in 70.53 µL) and then diluted into stapling buffer (973 µL for 7, NH_4HCO_3, 100 mM, pH= 8). TCEP was dissolved at 100x the final concentration in water (20 mM) and added to the stapling reaction (2 eq., 14.1 µL). α,α-Dibromo-m-xylene was dissolved at 4x the final concentration in MeCN (500 µM) and then added (1.25 eq., 353 µL for HeloMYC-711) to the protein in stapling buffer. Final concentrations used were 100 µM (1 eq.) protein, 125 µM (1.25 eq.) staple and 200 µM (2 eq.) TCEP. Final MeCN content was 25%.

When the stapling reaction was completed as seen by LC-MS the product was purified using a Biotage® Selekt Flash Purification System equipped with a Biotage® Sfär C18 D - Duo 10 g column on a gradient of water in MeCN (0-100%,with a flat gradient between 15% and 79%), both containing 0.1% TFA. The product containing fractions were lyophilized yielding the proteins as TFA salts.

Yield HeloMYC-37 (**10**): 0.27 mg (38%)

Yield HeloMYC-711 (**11**): 0.32 mg (26%)

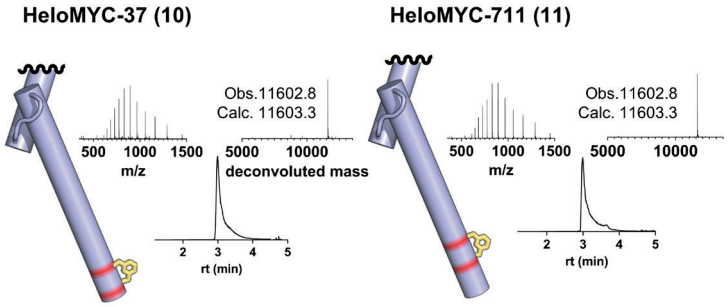

4.6.2.1.3 Cys-capping of 4 with benzyl bromide

Protein **4** (2.8 mg, 202 nmol, 1eq.) was dissolved at 20x the final concentration in water (101 µL, 2 mM) and then diluted into stapling buffer (NH_4HCO_3, 100 mM, pH= 8). Benzyl bromide was dissolved at 4x the final concentration in MeCN (1 mM) and then added to the protein in stapling buffer (505 µL, 2.5 eq.). Final concentrations used were 100 µM (1 eq.) for the protein and 250 µM (2.5 eq.) for benzyl bromide. Final MeCN content was 25%.

When the stapling reaction was completed as seen by LC-MS the product was purified using a Biotage® Selekt Flash Purification System equipped with a Biotage® Sfär C18 D - Duo 10g column on a gradient of water in ACN, both containing 0.1% TFA. The product containing fractions were lyophilized yielding BenzoMYC (**S1**) (1.06 mg, 75 nmol, 37%) as TFA salt. In addition to the main peak which corresponds to the desired product, a second deconvoluted mass corresponding to an additional benzyl substitution is detected in the product.

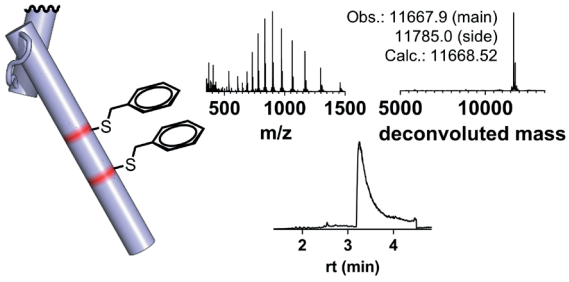

4.6.2.2 FITC labelling

4.6.2.2.1 Labelling Omomyc

Omomyc (4.19 mg, 300 nmol, 1 eq.) was dissolved in carbonate buffer (0.1 M, pH 9.1,

4.19 mL) to a concentration of 1 mg/mL and cooled to 0 °C. Subsequently, a solution of FITC in dmso (1.7 mM, 159 µg, 240 µL, 408 nmol, 1.36 eq.) was added slowly over the course of approximately 4 h. The crude product was then purified by reverse phase column chromatography using a Biotage® Selekt Flash Purification System with a Biotage® Sfär C18 D - Duo 100 Å 30 µm column 10 g applying a gradient of 0-100% MeCN in water (0-100% with a flat gradient between 20% and 48%) yielding FITC-labelled Omomyc-F (12) (0.93 mg, 65 nmol, 22%) as TFA salt after lyophilization.

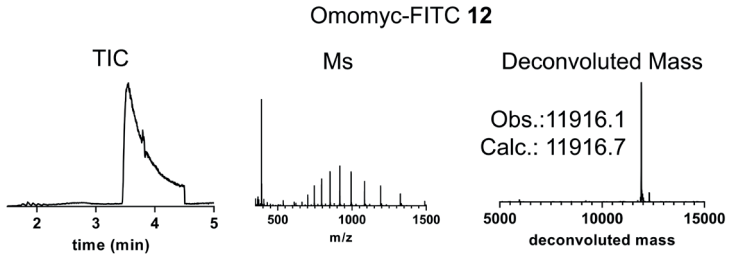

LC-MS spectrum with total ion count, extracted ion count and deconvoluted mass of FITC-labelled OmoMyc (**12**).

4.6.2.2.2 Labelling HeloMYC-1421

HeloMYC-1421 (1.35 mg, 96 nmol, 1 eq.) was dissolved in carbonate buffer (0.1 M pH 9.1, 1.35 mL) to a concentration of 1mg/mL and cooled to 0°C. Subsequently, a solution of FITC in dmso (1.56 mM, 67.7 µL, 106 nmol, 1.1 eq.) was added over the course of 4.5 h. The crude product was then purified by reverse phase column chromatography using a Biotage® Selekt Flash Purification System with a Biotage® Sfär C18 D - Duo 100 Å 30 µm column 10 g applying a gradient of 0-100% MeCN in water (0-100% with a flat gradient between 20% and 48%), yielding FITC-labelled HeloMYC-1421-F (**13)** (0.59 mg, 41 nmol, 43%) after lyophilization.

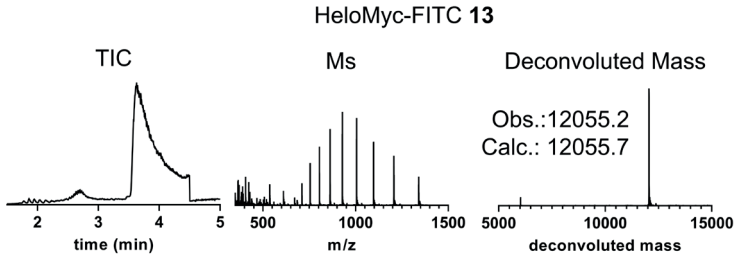

LC-MS spectrum with total ion count, extracted ion count and deconvoluted mass of FITC-labelled HeloMyc-1421 (**13**).

4.6.2.2.3 Synthesis of probe 18

Fmoc-Rink-amide-Protide resin (100 mg, 0.6 mmol/g loading) was incubated with piperidine (20% in DMF, 2 mL) for 10 minutes and then washed with DMF (5 x 3 mL). A HATU solution in DMF (0.4 M) was prepared and each amino acid building block was dissolved in this solution (appropriate amount to result in final amino acid concentration of 0.4 M, 500 µL). For each coupling cycle DIPEA (100 µL) was added to the amino acid HATU mix (500 µL) for preactivation. After 30 seconds this solution was added to the resin, stirred and then incubated for 15 minutes. The coupling mixture was drained under vacuum and the resin washed with DMF (3 x 3 mL), before Fmoc removal with piperidine (20% in DMF, 2 mL) for 10 minutes followed by washes with DMF (5 x 3 mL). As last linear building block we incorporate Fmoc-Lys(Biotin)-OH, followed by Fmoc removal. The peptide was then acetylated via treatment with acetic anhydride (10% in DMF with 10% DIPEA, 2 mL, 10 minutes). After washes with DMF (5 x 3 mL) and CH_2Cl_2 (3 x 3 mL), the resin was incubated with TFA (1% in CH_2Cl_2, 1 mL, 5 x 2 min) to remove the Mmt protecting group. Dibromomaleimide-hexanoic acid (74 mg) was dissolved in DMF containing 0.4 M HATU (500 µL), activated with DIPEA (100 µL) and then added to the peptidyl resin and incubated for 30 minutes. The resin was washed with DMF (5 x 3 mL) and CH_2Cl_2 (3 x 3 mL) before cleavage and global deprotection with TFA + 5% water, 60 minutes. The probe was precipitated with ice cold ether analyzed by LCMS and used without further purification.

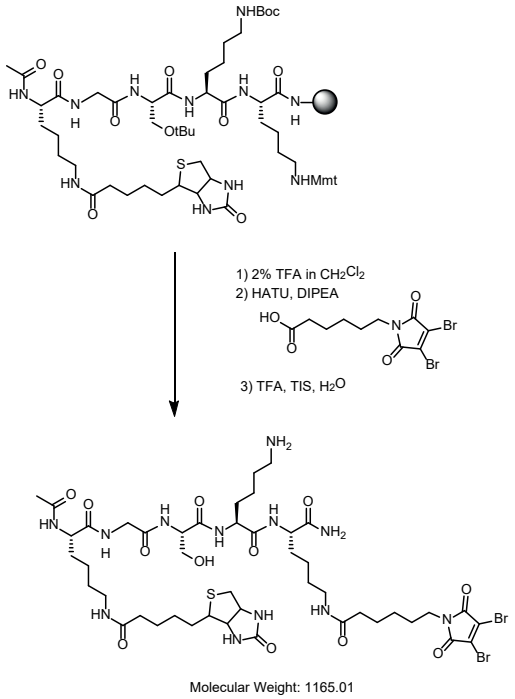

Molecular Weight: 1165.01

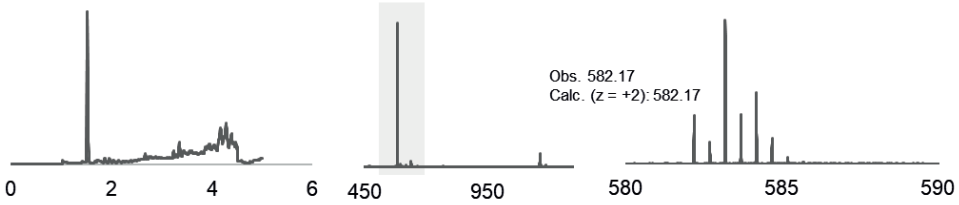

LCMS trace and spectrum of probe 18.

4.6.2.2.4 Synthesis of probe 19

The synthesis follows the same procedure as detailed above. As last linear building block JQ1-acid was incorporated, under the same coupling conditions as detailed for all amino acid building blocks.

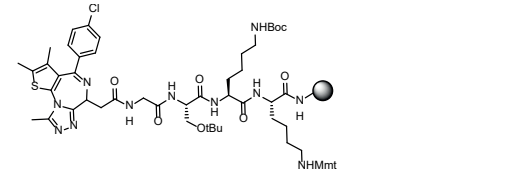

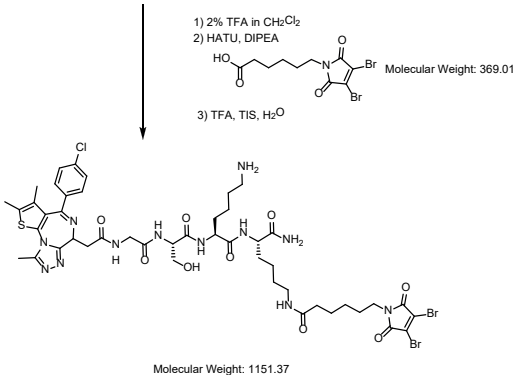

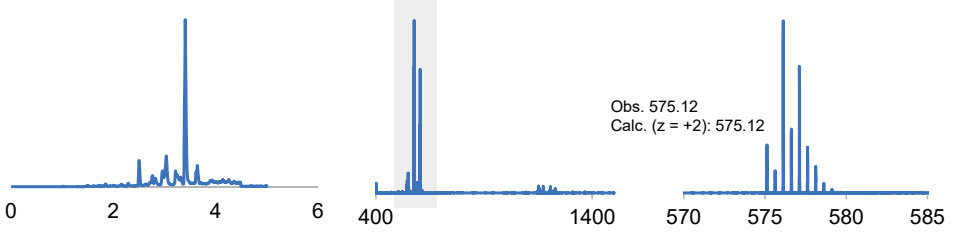

LCMS trace and spectrum of probe 19.

4.6.2.2.5 Synthesis of protein conjugates 20 and 21

The protein (2 mg, 140 nmol) was dissolved in stapling buffer (500 µL, NH_4HCO_3, 100 mM, pH= 8), and then diluted with MeCN (250 µL). TCEP was dissolved in water (20 mM) and added to the stapling reaction (2 eq., 14.0 µL). Probe (18 or 19) was dissolved in MeCN (10 mM) and then added (2 eq., 28 µL) to the protein in stapling buffer. The reaction was incubated for 60 min. When the stapling reaction was completed as determined by LC-MS the product was purified using a size exclusion (cut off 7 kDa) zeba spin column.

4.6.3 Protein expression and characterization

4.6.3.1 Site-directed mutagenesis

For site-directed mutagenesis the QuikChange II site-directed mutagenesis kit (Agilent Technologies) was used and primers were designed using the QuikChange® Primer Design Program provided by Agilent Technologies. Mutagenesis was performed according to the manufacturer's protocol In brief, PCR reactions were prepared using pET-30a with Omomyc as template (0.5 µL, ~25 ng), forward and reverse primers (0.6 µL each, 10 µM), MQ water (18.8 µL) as well as the contents provided by the kit: NTP mix (1 µL), 10x reaction buffer (2.5 µL) and *PfuUltra* high fidelity DNA polymerase. In some cases, when the formation of primer dimers was seen, primer concentration was reduced and 1 µL of dmso was added. PCR was performed for 22 cycles (95 °C, 30s; 55 °C, 1 minute; 68 °C, 10 minutes) followed by *Dpn I* restriction for 2 hours at 37 °C (addition of 0.5 µL at 10 U/µL)

Mutated plasmids were then incorporated into XL-1 blue competent cells. Cells were thawed on ice and 8 µL of the *Dpn I*-treated DNA were added to 50 µL of cells. The mixture was incubated on ice for 30 minutes, followed by a 45 second heat pulse at 42 °C and incubation on ice for another 2 minutes. Subsequently, 0.5 mL SOC-medium were added and the cells shaken at 250 rpm, 37 °C for 1 hour. For selection, 100 µL of the mixture were plated on one half of an LB agar plate containing gentamicin and kanamycin. The rest of the cells was spun down, the supernatant removed except for 100 µL, the cells resuspended in these 100 µL and plated on the other half of the LB agar plate. The plate was incubated at 37 °C overnight.

About 5-10 colonies were picked from selection and grown overnight in 5 mL LB media supplemented with gentamicin and kanamycin and plasmid DNA was isolated using the QIAprep Spin Miniprep kit (Qiagen, Venlo, NL) according to the manufacturer's protocol. The isolated plasmid DNA was sequenced using a sanger sequencing service and analyzed using Benchling.

4.6.3.2 Primers used for site-directed mutagenesis

Mutation	Primer sequence 5'-3' (forward, mutation in bold)
C91A	caaacttgaacagctacggaactct**gct**gcgtaaggactc
T3C	gatatcggatccatggcg**tg**cgaggagaatgtcaagag
V7C	ccatggcgaccgaggagaat**tg**caagaggcgaacac
V7C T11C	ggcgaccgaggagaat**tg**caagaggcga**tgc**cacaacgtcttggagc
V14C	gaggcgaacacacaac**tg**cttggagcgccagagg
N21C	gagcgccagaggagg**tg**cgagctaaaacggag

4.6.3.3 Primers used for sequencing

Name	Sequence 5'-3'
T7 terbis – sequencing reverse	aacccctcaagacccg
pET upstream – sequencing forward	gatgcgtccggcgtagag

4.6.3.4 Expression of different Omomyc variants

Plasmids used were either obtained from site-directed mutagenesis of pET-30a with the omomyc gene sequence (for stapled variants termed HeloMYC) or genes as well as insertion of them by express cloning were ordered from GenScript and the plasmids used as delivered (for artificial coiled-coil and mutations in the coiled-coil termed ArtiMYC and ArgiMyc as well as NLS-HeloMYC fusions, see annex for plasmid sequences).

Plasmids were transformed into competent ArcticXpress DE3 RIL cells by heat shock according to the manufacturer's protocol. Briefly, 2 µL of 10% β mercaptoethanol were mixed with 100 µL of competent cell suspension thawed on ice and incubated for 10 minutes on ice. Next, 25 ng of plasmid DNA were added and the cells incubated for another 30 minutes on ice. The cells were then heat-shocked in a water bath for 20 seconds at 42 °C and subsequently incubated on ice for 2 minutes followed by the addition of 0.9 mL SOC media and incubation at 37 °C and 250 rpm for 1 h. Cells were then pelleted by centrifugation, 0.9 mL of the supernatant decanted and the pellet resuspended in the remaining 100 µL of media. Cells were plated for selection on LB agar with kanamycin and gentamicin and incubated at 37 °C overnight.

Single colonies were picked from the plate and cultured overnight at 37 °C and 180 rpm in 100 mL of LB media containing kanamycin and gentamycin. Next, 3x2 L of LB media containing kanamycin and gentamycin in 5 L Erlenmeyer flasks were inoculated with 25 mL of preculture and grown at 37 °C and 180 rpm until an OD of 0.8 was reached. The temperature was then set to 14 °C and protein expression

induced by addition of IPTG to a final concentration of 100 µM. Protein expression was conducted overnight for 18 h after which the cells were harvested by centrifugation (5,000g, 4 °C, 12 min.), the pellet resuspended in lysis buffer (20 mM Tris-HCl pH 8, 0.5 M NaCl, 10 mM imidazole, 3 mM $MgCl_2$, freshly added 1 cOmplete EDTA-free protease inhibitor cocktail tablet per 50 mL of buffer and 0.05-0.1% DNase) and the cells lysed by pressure lysis. Cell debris was removed by ultracentrifugation (35,000 rpm, 4℃, 45 min.)

4.6.3.5 Purification of His-tagged proteins

After ultracentrifugation, the supernatant was purified using an ÄKTA start protein purification system equipped with a 5 mL HisTrap HP His-tag protein purification column (Cytiva). After washing out unbound protein with wash buffer (20 mM Tris-HCl pH 8, 0.5 M NaCl, 10 mM imidazole) the protein was eluted using a gradient of 10 mM to 500 mM imidazole in the same buffer over 40-50 column volumes of buffer. Fractions with protein were analyzed for protein content and identity by LC-MS.

4.6.3.6 General protocol for buffer exchange

The combined fractions obtained from Ni-column purification were incubated with 5 mM TCEP for 1h to break any possible formed disulfide bonds. The buffer was then exchanged by subjecting the protein to column chromatography on a Biotage® Selekt Flash Purification System equipped with a Biotage® Sfär C18 D - Duo 25g or 50g column and a stepwise gradient of 0 % MeCN in water followed by 50 to 100% MeCN in water). The combined fractions containing the protein were lyophilized, yielding the His-tagged or final protein as TFA salt.

4.6.3.7 Tag cleavage with enterokinase and subsequent purification

Lyophilized protein was dissolved at 2 mg/mL in EK cleavage buffer (200 mM Tris-HCl, pH 7.4, 0.5 M NaCl, 20 mM $CaCl_2$) and after addition of 10 u/mL enterokinase the protein was incubated overnight. The protein was then purified using an ÄKTA start protein purification system equipped with a 5 mL HisTrap HP His tag protein purification column (Cytiva) applying a gradient of 10 mM to 500 mM imidazole in elution buffer (20 mM Tris-HCl pH 8, 0.5 M NaCl, 10-500 mM imidazole). The fractions were analyzed by LC-MS and the buffer of the combined protein containing fractions was exchanged as described above, yielding the final proteins as TFA salts after lyophilization.

4.6.3.8 Electromobility shift assay (EMSA)

For EMSAs, proteins were serial diluted with water to a final volume of 10 µL. Subsequently, 5 µL of 4x EMSA buffer (final buffer concentration: 20 mM HEPES

pH 8.0, 150 mM NaCl, 5% glycerol, 1 mM EDTA, 2 mM $MgCl_2$, 0.5 mg/mL of BSA, 1 mM DTT and 0.05% NP-40) followed by 5 µL of 4x FAM-labelled DNA construct (IRD700-ACC CCA CCA CGT GGT GCC T, final concentration 4 nM) were added.

The samples were incubated for 30 minutes at room temperature, placed on ice and incubated for another 15 minutes. Then 15 µL of the samples were loaded onto a 10% native acrylamide TBE gel which was pre run before for 1 h at 75 V at 4 °C in 0.5x TBE. Samples were run for 20 minutes at 120 V followed by 40 minutes at 100 V at 4 °C in 0.5x TBE and subsequently scanned on a Bio-Rad ChemiDoc MP machine. Bound protein signal was quantified using ImageJ and KD values were obtained using the inhibitor concentration vs. response variable slope model of nonlinear regression in GraphPad Prism 9.0.0.and the IC50 value reported as KD.

4.6.3.9 Circular Dichroism Spectroscopy

For CD measurements 1 mM protein stocks were diluted to 20 µM in Dulbecco's phosphate buffered saline (DPBS) to a final volume of 200 µL. For DNA containing samples, a 1 mM DNA stock in water was heated for 5 min to 95 °C, let cool down to RT and an equimolar amount of DNA was added to the protein samples dedicated to be measured with DNA. Additionally, a blank measurement with or without DNA was measured. Circular Dichroism (CD) samples were measured at 37 °C using a Jasco J-8151 CD spectrometer with a 1 mm path length quartz cuvette. The following parameters were used for a full wavelength scan: wavelength = 260-200 nm; Data pitch = 1 nm; scanning mode = continuous; scanning speed = 100 nm/min; response = 1, BW = 1, accumulation = 5. For CD melting curves the same samples were cooled down to 5 °C and slowly heated to 90 °C while measuring at 222 nm, with a heating speed of 2 °C/min.

For CD analysis, the blank measurement was subtracted from each spectrum and the mean residue molar ellipticity (θ, deg cm^2 dmol) was calculated using the following equation[2]:

$$\left[\emptyset\right] = \frac{100*\emptyset_{obs}}{c*n*l}$$

With θ_{obs} in mdeg, concentration (c) in mM, peptide bonds (n) and path length of cuvette in cm.

4.6.3.10 Serum stability assay

For serum stability assays 1 mM protein stocks were diluted to a final concentration of 60 µM in 10% human serum in DPBS. The mixture was vortexed immediately after protein addition and 5 µL aliquots were mixed with 5 µL of 20% TFA in water (t = 0) to quench the human serum, resulting in protein precipitating. Subsequently, the protein

serum solution was incubated at 37 °C using a BIO-RAD T100™ Thermal Cycler with the lid set to 95 °C. At indicated timepoints 5 µL aliquots were mixed with 5 µL of 20% TFA in water. The resulting pellet was then diluted 5.5x with additional DPBS to redissolve. This solution was analyzed according to the high resolution LCMS protocol (Method C). As internal standard (IS), the extracted-ion chromatogram (XIC) from m/z = 1233.52 was used belonging to human serum albumin. After measurement, the XIC obtained from the highest intensity peak belonging to each protein and IS were extracted from the total-ion chromatogram (TIC). Using Graphpad Prism 9, the area under the curve (AUC) from each timepoint was calculated, normalized against the AUC of the IS followed by normalization against t = 0 and plotted. Next, a nonlinear regression – One phase decay analysis was performed to obtain $t_{½}$ with a plateau constant equal to 0 and Y_0 set to 1. The assay was performed in triplicates. For Omomyc one set of outliers in the measurement was excluded.

4.6.3.11 Cell culture and cell assays

Cells were cultured at 37°C in 5% CO_2 atmosphere. Cell lines were cultured in ATCC recommended media and split twice a week before confluency was reached.

4.6.3.12 MYC reporter gene assay

The reporter gene assay was performed using Cignal reporter assay (CCS-012L, Qiagen) according to the manufacturer's protocol. In brief, HEK293T cells were harvested and resuspended in OptiMEM media containing 5% FBS and 1% non-essential amino acids (NEAA) as well as penicillin/streptavidin. 40,000 cells were seeded per well in a 96-well plate and 50 µL transfection cocktail of either cignal reporter or positive or negative control reporter along with attractene transfection reagent in OptiMEM without additives was added and the cells incubated overnight. Next, media was changed to assay media (OptiMEM, 0.5% FBS, 1% NEAA, penicillin/streptavidin) and the cells were incubated for 8 hours after which the media was replaced by 75 µL assay media containing the different proteins at the required concentration and the cells were incubated with the proteins for 24 hours.

Luciferase assay was then performed using a luciferase assay kit (E2940, Promega). Cells were lysed by addition of 75 µL of DualGlo luciferase assay reagent and incubated for 15 minutes after which Luciferase luminescence was measured on a Perkin Elmer EnVision 2104 Multilabel Reader. Subsequently, 75 µL of DualGlo Stop & Glo reagent were added and the renilla luciferase luminescence measured after 15 minutes of incubation time.

Signal was normalized against cell number by calculating the ratio of firefly and renilla luminescence and eventually these signals were normalized against the untreated control. All experiments were done in technical triplicates. Data was analyzed using

GraphPad Prism 9.0.0. applying the model of inhibitor concentration vs. response with variable slope model for nonlinear regression.

4.6.3.13 MYC reporter assay control for direct luciferase inhibition

For the control experiment testing direct luciferase inhibition by proteins, the cells were incubated for 24 hours in assay media and the media replaced by assay media containing the proteins directly before performing the luciferase assay as described above.

4.6.3.14 Cell proliferation assay

Cells were seeded in 100 µL of their respective media at 1500 cells/well (Figure 5.5d) or 2000 cells/well (Figure 5e) in a white opaque 96-well plate and let attach overnight. Media was then changed to 100 µL of media with the required protein at the appropriate concentration, the plate was covered with a membrane to prevent media evaporation and the cells were incubated with the proteins for 72 hours. Cell proliferation was then assessed using CellTiter-Glo (Promega) reading luminescence on a Perkin Elmer EnVision 2104 Multilabel Reader. All experiments were done in technical triplicates. Data was analyzed using GraphPad Prism 9.0.0.

4.6.3.15 Live cell microscopy with FITC-labelled HeloMYC and Omomyc

Hela cells were harvested and seeded at 12'000 cells/well in a 96-well plate and left to adhere overnight (4.5h in the case of 24h compound treatment). Cells were then treated with 5µM Omomyc-FITC (12) or HeloMYC-1421-FITC (13) for the desired time in full media. Subsequently, the media was aspirated cells were stained for 10 minutes with 1µg/mL Hoechst in DPBS, followed by three washes with full media. Live cells were imaged on a Nikon Ti2 microscope equipped with a Plan Apo VC 20x DIC N2 air objective using a 405nm laser for Hoechst and a 488nm laser for fluorescein excitation.

4.6.3.16 Quantification of signal in the green channel

For signal quantification the Hoechst channel was used and ROIs were determined by thresholding from 100-255. The ROIs were then dilated by 5 units to also cover the area surrounding the nucleus and a mask was created. The mask was applied to the FITC channel and the mean fluorescence measured per image. For each condition the mean of the mean fluorescence of the no treatment control was subtracted from the individual mean fluorescence and the values normalized to the desired condition.

4.6.3.17 RNA sequencing and GSEA

In a 12-well plate 50,000 HeLa cells/well were seeded. The next day the cells were treated with either 10 µM HeloMYC-1421 or vehicle in MEM media supplemented with 10% FBS, 1% Pen/Strep and Glutamax and incubated for 72 hours. Total RNA was isolated using Qiagen RNeasy Plus mini kit and dissolved in RNAse free water. Samples were shipped to and sequencing as well as differential gene expression analysis was performed by Novogene GmbH (Planegg, Germany). Gene set enrichment analysis (GSEA) was performed with the GSEA desktop application (Broad Institute) version 4.4.0 performing 10,000 permutations.

4.6.4 Protein sequences

Enterokinase cleavage sites shown with |

Omomyc MHHHHHHSSGLVPRGSGMKETAAAKFERQHMDSPDLGTDDDDK|AMADIGSMATEENVKRRTHNVLERQRRNELKRSFFALRDQIPELENNEKAPKVVILKKATAYILSVQAETQKLISEIDLLRKQNEQLKHKLEQLRNSCA

Omomyc T3C V7C C91A HHHHHHSSGLVPRGSGMKETAAAKFERQHMDSPDLGTDDDDK|AMADIGSMA**C**EEN**C**KRRTHNVLERQRRNELKRSFFALRDQIPELENNEKAPKVVILKKATAYILSVQAETQKLISEIDLLRKQNEQLKHKLEQLRNS**A**A

Omomyc V7C T11C C91A MHHHHHHSSGLVPRGSGMKETAAAKFERQHMDSPDLGTDDDDK|AMADIGSMATEEN**C**KRR**C**HNVLERQRRNELKRSFFALRDQIPELENNEKAPKVVILKKATAYILSVQAETQKLISEIDLLRKQNEQLKHKLEQLRNS**A**A

Omomyc V7C V14C C91A MHHHHHHSSGLVPRGSGMKETAAAKFERQHMDSPDLGTDDDDK|AMADIGSMATEEN**C**KRRTHN**C**LERQRRNELKRSFFALRDQIPELENNEKAPKVVILKKATAYILSVQAETQKLISEIDLLRKQNEQLKHKLEQLRNS**A**A

Omomyc V14C N21C C91A MHHHHHHSSGLVPRGSGMKETAAAKFERQHMDSPDLGTDDDDK|AMADIGSMATEENVKRRTHN**C**LERQRR**C**ELKRSFFALRDQIPELENNEKAPKVVILKKATAYILSVQAETQKLISEIDLLRKQNEQLKHKLEQLRNS**A**A

Omomyc Q64R D71R Q86R C91A - ArgiMyc MHHHHHHSSGLVPRGSGMKETAAAKFERQHMDSPDLGTDDDDK|AMADIGSMATEENVKRRTHNVLERQRRNELKRSFFALRDQIPELENNEKAPKVVILKKATAYILSVQAET**R**KLISEI**R**LLRKQNEQLKHKLE**R**LRNS**A**A

ArtiMyc MHHHHHHSSGLVPRGSGMKETAAAKFERQHMDSPDLGTDDDDK|AMADIGSMATEENVKRRTHNVLERQRRNELKRSFFALRDQIPELENNEKAPKVVILKKATAYILSV**KREIAALKREIAALKREIAALKRE**

NucleoMYC 16 MHHHHHHSSGLVPRGSGMKETAAAKFERQHMDSPDLGTDDDDK|AMADIG-SMATEENVKRRTHN**C**LERQRR**C**ELKRSFFALRDQIPELENNEKAPKVVILKKATAYILSVQA-ETQKLISEIDLLRKQNEQLKHKLEQLRNS**AA**P**AAKRVKLD**

NucleoMYC 17 MHHHHHHSSGLVPRGSGMKETAAAKFERQHMDSPDLGTDDDDK|AMADIG-S**PAAKRVKLD**MATEENVKRRTHN**C**LERQRR**C**ELKRSFFALRDQIPELENNEKAPKVVILKKA-TAYILSVQAETQKLISEIDLLRKQNEQLKHKLEQLRNS**A**A

4.6.5 Overview of all produced miniproteins

Protein	Sequence	Yield[1]	Molecular weight calculated	Molecular weight observed
Omomyc (**1**)	AMADIGSMATEENVKRRTHNVLERQRRNELKRSFFALRDQIPELENNEKAPKVVILKKATAY-ILSVQAETQKLISEIDLLRKQNEQLKHKLEQLRNSCA	13.7 mg/L 4.5 mg/L	11527.3	11526.6
ArgMYC (**2**)	AMADIGSMATEENVKRRTHNVLERQRRNELKRSFFALRDQIPELENNEKAPKVVILKKATAY-ILSVQAETRKLISEIRLLRKQNEQLKHKLERLRNSAA		11592.5	11591.8
ArtiMYC (**3**)	AMADIGSMATEENVKRRTHNVLERQRRNELKRSFFALRDQIPELENNEKAPKVVILKKATAY-ILSVKREIAALKREIAALKREIAALKRE	8 mg/L	10398.2	10397.6
Protein **4**	AMADIGSMATEENVKRRTHNCLERQRRCELKRSFFALRDQIPELENNEKAPKVVILKKATAY-ILSVQAETQKLISEIDLLRKQNEQLKHKLEQLRNSAA	20.9 mg/L 10.4 mg/L	11488.3	11487.7
Protein **5**	AMADIGSMATEENCKRRTHNCLERQRRNELKRSFFALRDQIPELENNEKAPKVVILKKATAY-ILSVQAETQKLISEIDLLRKQNEQLKHKLEQLRNSAA	6.2 mg/L	11503.3	11502.6
Protein **6**	AMADIGSMACEENCKRRTHNVLERQRRNELKRSFFALRDQIPELENNEKAPKVVILKKATAY-ILSVQAETQKLISEIDLLRKQNEQLKHKLEQLRNSAA	7.3 mg/L 2.3 mg/L	11501.3	11500.6
Protein 7	AMADIGSMATEENCKRRCHNVLERQRRNELKRSFFALRDQIPELENNEKAPKVVILKKATAY-ILSVQAETQKLISEIDLLRKQNEQLKHKLEQLRNSAA	8 mg/L 4.4 mg/L	11501.3	11500.6
HeloMYC-1421 (**8**)	AMADIGSMATEENVKRRTHNCLERQRRCELKRSFFALRDQIPELENNEKAPKVVILKKATAY-ILSVQAETQKLISEIDLLRKQNEQLKHKLEQLRNSAA (stapled with 1)	69%	11666.3	11665.8
HeloMYC-714 (**9**)	AMADIGSMATEENCKRRTHNCLERQRRNELKRSFFALRDQIPELENNEKAPKVVILKKATAY-ILSVQAETQKLISEIDLLRKQNEQLKHKLEQLRNSAA (stapled with 1)	67%	11681.3	11680.8
HeloMYC-37 (**10**)	AMADIGSMACEENCKRRTHNVLERQRRNELKRSFFALRDQIPELENNEKAPKVVILKKATAY-ILSVQAETQKLISEIDLLRKQNEQLKHKLEQLRNSAA (stapled with 2)	28%	11603.3	11602.8
HeloMYC-711 (**11**)	AMADIGSMATEENCKRRCHNVLERQRRNELKRSFFALRDQIPELENNEKAPKVVILKKATAY-ILSVQAETQKLISEIDLLRKQNEQLKHKLEQLRNSAA (stapled with 2)	26%	11603.3	11602.8
Omomyc-FITC (**12**)	AMADIGSMATEENVKRRTHNVLERQRRNELKRSFFALRDQIPELENNEKAPKVVILKKATAY-ILSVQAETQKLISEIDLLRKQNEQLKHKLEQLRNSCA*FITC	22%	11916.7	11916.1
HeloMYC-FITC (**13**)	AMADIGSMATEENVKRRTHNCLERQRRCELKRSFFALRDQIPELENNEKAPKVVILKKATAY-ILSVQAETQKLISEIDLLRKQNEQLKHKLEQLRNSAA*FITC (stapled with 1)	43%	12055.7	12055.6
BenzoMYC (**S1**)	AMADIGSMATEENVKRRTHNCLERQRRCELKRSFFALRDQIPELENNEKAPKVVILKKATAY-ILSVQAETQKLISEIDLLRKQNEQLKHKLEQLRNSAA (Cys-capped with Bz)	37%	11668.5	11667.9
NucleoMYC (**16**)	ADIGSMATEENVKRRTHNCLERQRRCELKRSFFALRDQIPELENNEKAPKVVILKKATAY-ILSVQAETQKLISEIDLLRKQNEQLKHKLEQLRNSAAPAAKRVKLD (stapled with 1)	60&	12645.2	12645.3
NucleoMYC (**17**)	ADIGSPAAKRVKLDMATEENVKRRTHNCLERQRRCELKRSFFALRDQIPELENNEKAPKV-VILKKATAYILSVQAETQKLISEIDLLRKQNEQLKHKLEQLRNSAA (stapled with 1)	46%	12645.2	12645.1

[1]First number represents yield of his-tagged protein, second number represents yield of tag-cleaved protein

4.7 Supplementary Figures

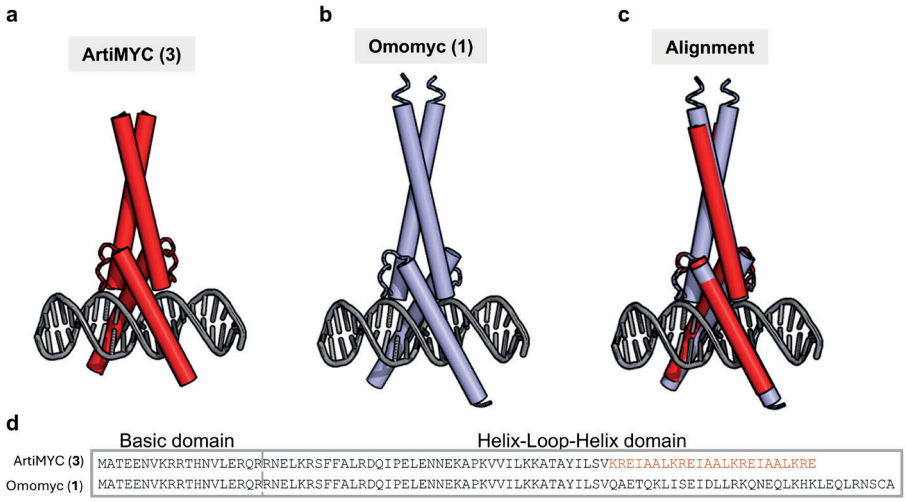

▲Figure S4.1. Folding of Omomyc (1) and ArtiMYC (3) is very similar. (**a-c**) Structures of ArtiMYC (**3**, a) and Omomyc (**1**, b) aligned (c). (**d**) The sequences of ArtiMYC (**3**) and Omomyc (**1**) with the artificial coiled-coil highlighted. Structure of ArtiMYC (**3**) was predicted using AlphaFold[1] and aligned to Omomyc (**1**) using Pymol. DNA shown in all panels is DNA from alignment with Omomyc (**1**).

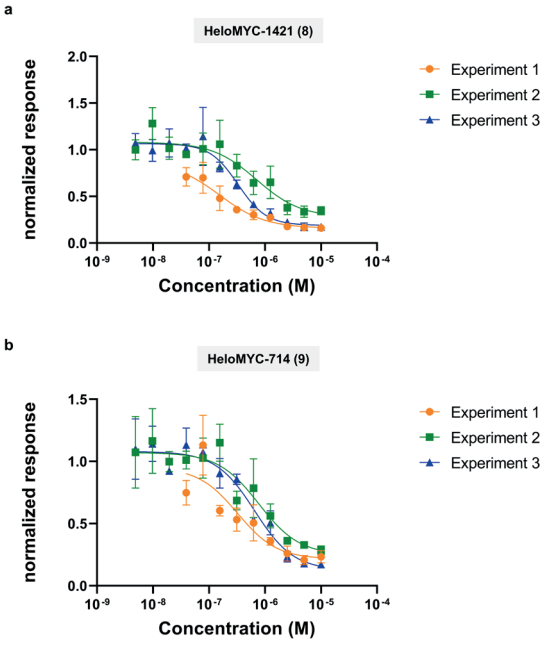

▲Figure S4.2. Results of three independent MYC reporter gene assay experiments to determine the EC_{50} of HeloMYC-1421 (**8**, **a**) and HeloMYC-714 (**9**, **b**). Results shown have no outliers removed and might differ slightly from the one curve shown in the main paper figure 4.4b.

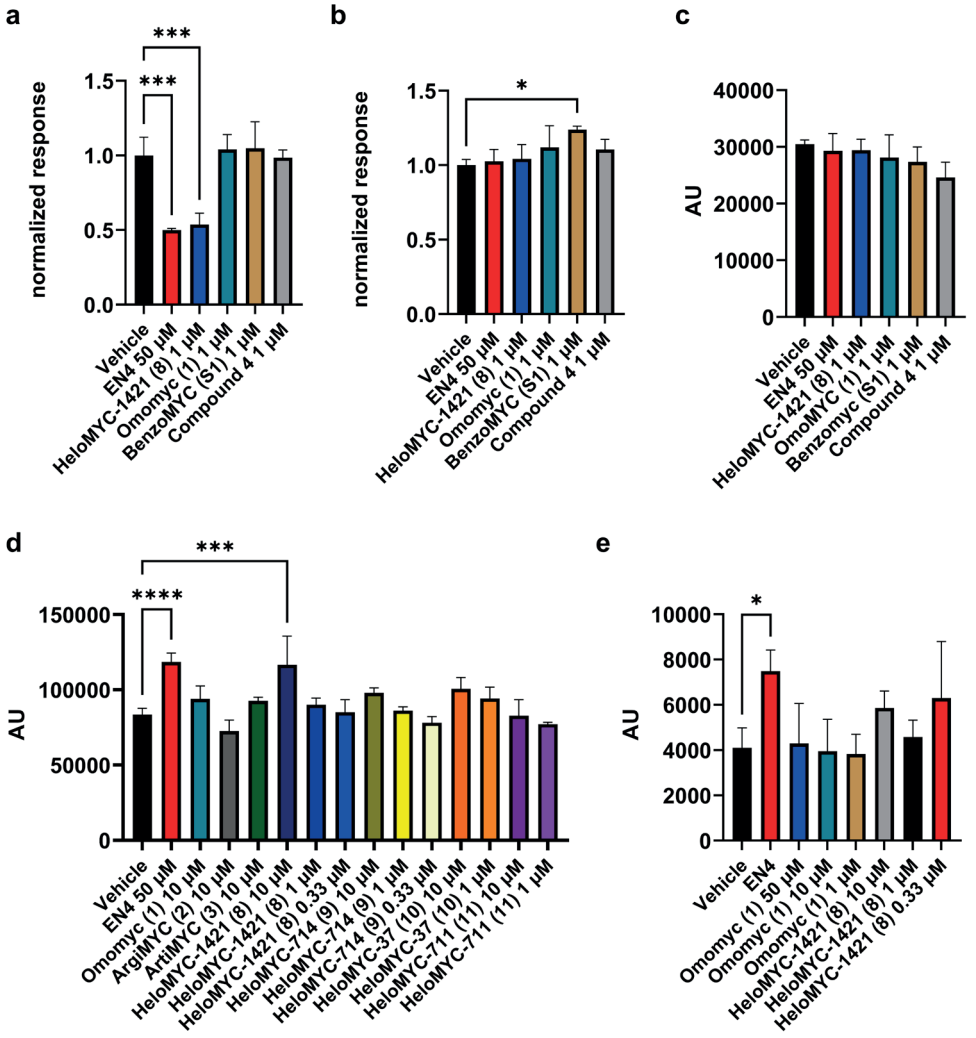

▲Figure S4.3. Control experiments to validate reporter gene assay data. (a) Positive control experiment shows effect of HeloMYC-1421 and EN4 on luciferase expression. HEK293T cells were transfected with a plasmid in which not only renilla luciferase expression but also firefly luciferase expression is under control of the CMV promoter instead of a MYC-responsive element. **(b)** Miniproteins are no direct luciferase inhibitors. HEK293T cells were transfected with the same plasmid as in panel a but treated with the indicated miniproteins shortly before cell lysis and addition of luciferase substrate to rule out any effect on gene transcription and expression. (**c-e**) Miniproteins have negligible effect on renilla luciferase expression under control of the CMV promoter. Shown is the renilla luciferase signal used for signal normalization of the experiments shown in figure S4.3a (panel c) and figure 4.4a and b (panels d and e, respectively) in the main text. Statistics**.** A one way ANOVA was performed to compare the effect of miniprotein treatment on firefly or renilla luciferase expression showing that there was a (a, b, d, e) or no (c) statistical difference between treatments (a) $F(5, 12) = 18.73$, $P<0.0001$; (b) $F(5, 12) = 3.115$, $P=0.0496$; (c) $F(5, 12) = 1.780$, $P=0.1915$; (d) $F(14, 30) = 8.662$, $P<0.0001$; (e) $F(7, 16) = 2.889$, $P=0.0373$.

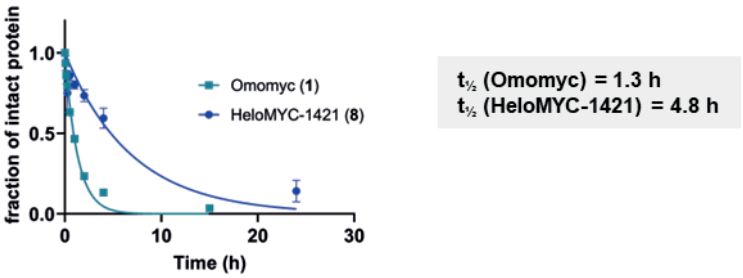

▲**Figure S4.4** HeloMYC-1421 displays improved serum stability compared to Omomyc.

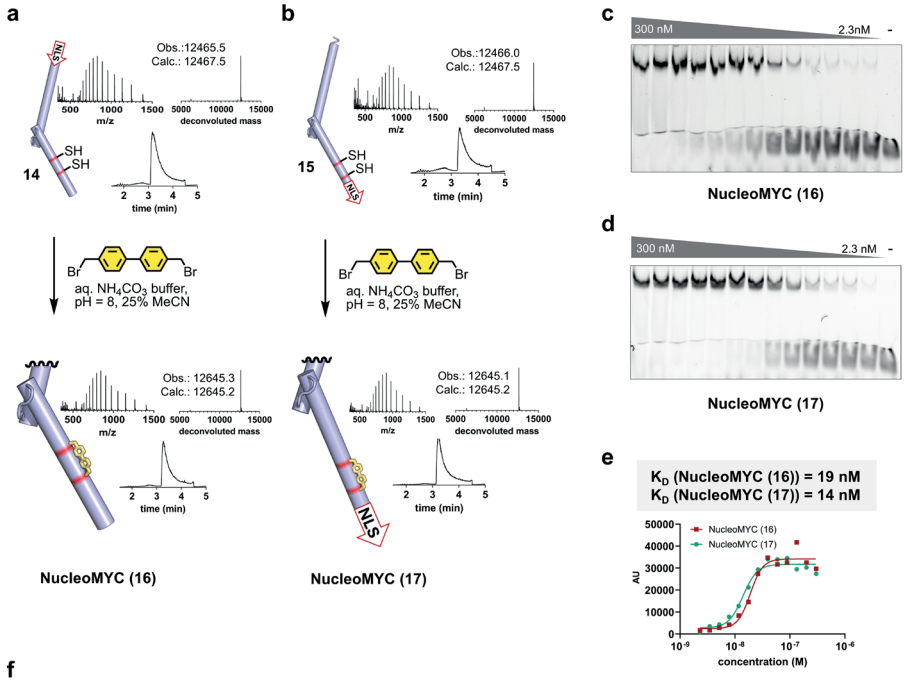

▲**Figure S4.5. NucleoMYC containing a nuclear localization sequence (NLS) fused to HeloMYC-1421 binds to E-Box DNA.** (**a, b**) An NLS sequence can be fused C- or N-terminally to the HeloMYC-1421 sequence, expressed and subsequently stapled, yielding NucleoMYC proteins **16** and **17**. (**c, d, e**) Both NucleoMYC proteins bind to E-BoxDNA in an EMSA with a K_D of 19 and 14 nM, respectively. (**f**) The sequence of NLS-containing NucleoMYC proteins.

4.8 References

1. Jumper, J. *et al.* Highly accurate protein structure prediction with AlphaFold. *Nature* **596**, (2021).

2. Crone, N. S. A., Kros, A. & Boyle, A. L. Modulation of Coiled-Coil Binding Strength and Fusogenicity through Peptide Stapling. *Bioconjug. Chem.* **31**, 834–843 (2020).